Chapter 3

Structural Ageing of a Cable-Stayed Bridge During Load-Test: The Overall Effect Monitored by Acoustic Emission

Giovanni P. Gregori, Giuliano Ventrice, Sebastiano Pinori, Genesio Alessandrini and Francesco Bianchi

Additional information is available at the end of the chapter

http://dx.doi.org/10.5772/54840

1. Introduction

A study is here presented, which was carried out on a steel bridge monitored by acoustic emission (AE), during load-test before its opening to public. Other standard security checks of linear deformation were simultaneously carried out, according to law requirements, by laser monitoring.

The focus of the present study is on material fatigue, consequent to load test. This newly constructed viaduct displayed an excellent performance. Hence, it is an effective and suitable reference to be compared with every old metal viaduct. In some respect, and up to some extent, this study also applies to concrete, or brick, or wood bridges. Indeed, fatigue is a permanently ongoing process and, when integrated over time, it affects old structures, causing progressive ageing and loss of performance and security. The difference between bridges constructed by different materials only relies on a different response-time to an applied tress. But fatigue and ageing are a much similar process when dealing with different materials. There is only need for a suitable calibration focused on every given case history.

The technique here applied relies on passive AE monitoring in the ultrasound band. AE are spontaneously released by every stressed solid material. Indeed, AE occur as a response to every gentle stress, independent of its cause.

It should be pointed out that AE intensity is not of concern for the analysis which is here considered. The only requirement is that an AE signal is detectable. The timing of the AE release, not the intensity, is rather fundamental for the present analysis.

Several applications of ultrasound monitoring are reported as a standard in the literature and they deal with several engineering concerns. However, the method, which is here applied for data handling, for analysis and for physical interpretation, derives from an original procedure[1] which is completely different compared to all previous procedures by other authors that are reported in the literature.

The viaduct of the present study is named "Cavalcaferrovia Ostiense" (i.e. "Overpass Ostiense"). It holds three-lanes (altogether *11.5 m* wide) in each direction, plus two large sidewalks. It connects the major road "Circonvallazione Ostiense", on its eastern side, with the arterial road "Ostiense" on its western side (figure 1). It is ~ *159 m* long, and is located in the Rome neighbourhood named Garbatella. Hence, it is here briefly called "Garbatella bridge" (figure 2, 3 and 4).[2] Its design reminds about a *3*-leg spider, with one "leg" on its eastern side. "Side A" is its northern side and "side B" its southern side. Each side is further distinguished, respectively, into its eastern (E) and western (W) segment (figures 3 and 4).

It crosses over a four-way railway, i.e. two ways of the Rome urban metro plus two ways of the suburban train Roma-Lido di Ostia. The height of the viaduct with respect to the railway[3] is comparable to the height of a train inside a standard railway tunnel. Every urban train always stops at the Garbatella station, which is very close to the viaduct (figure 1), while every suburban train crosses through it at moderate, although sometimes low, speed.

Thermal dilatation is compensated at the two western "legs" of the bridge that can slide longitudinally, while the single eastern "leg" is fixed to its concrete basement.

AE monitoring was implemented on *December 16th, 2011* on the occasion of the load test,[4] which was formally carried out on *December 17th, 2011*.[5] The total load was made by means of *28* mobile concrete mixers, filled with rubble, everyone of total weight of ~ 3.5 tons. Altogether the load was 9800 kN.

The load test was exploited in four steps. During *Step 1* the load was symmetric (*14* mixers on each side A and B). *Step 2* was asymmetric with *14* mixers on side A and no mixer on side B. *Step 3* was carried out with *5* mixers over segment A-E and *5* mixers over segment B-W. *Step 4* had a load of *8* mixers over segment A-E and *8* mixers over segment B-E.

Standard monitoring was exploited by means of laser measurements concerning several linear deformations to be compared with model computation. In addition, model computations also

1 The algorithms that are here applied include a few methods that already appeared in a few papers by the authors and co-workers (see below). These procedures are now also a part of a more systematic and compact set of methods for technological applications, which were implemented and patented by G. P. Gregori. Their practical exploitation and applications are in progress at S.M.E.

2 The design is by "Solidus srl – Ing. Francesco Del Tosto", with components provided by "Cimolai spa",Pordenone, Italy.

3 The road level with respect to the highest side of the rail is 7.80 m. We acknowledge and thank Ing. Francesco del Tosto for providing us with this (and other) information.

4 We acknowledge Ing. Fabio Rocchi for kindly providing with the official documentation.

5 The legal prescriptions are specified by the Italian Ministerial Decree D.M. LL. PP. 14/01/2008, Technical standards for construction, and by its explanatory supplement 02/02/2009, n. 617, Instructions for the application of the "Technical standards for construction" (D.M. 14 January 2008).

http://dx.doi.org/10.5772/54840

specify the axial stress of several different components of the bridge, which were compared with direct measurements.

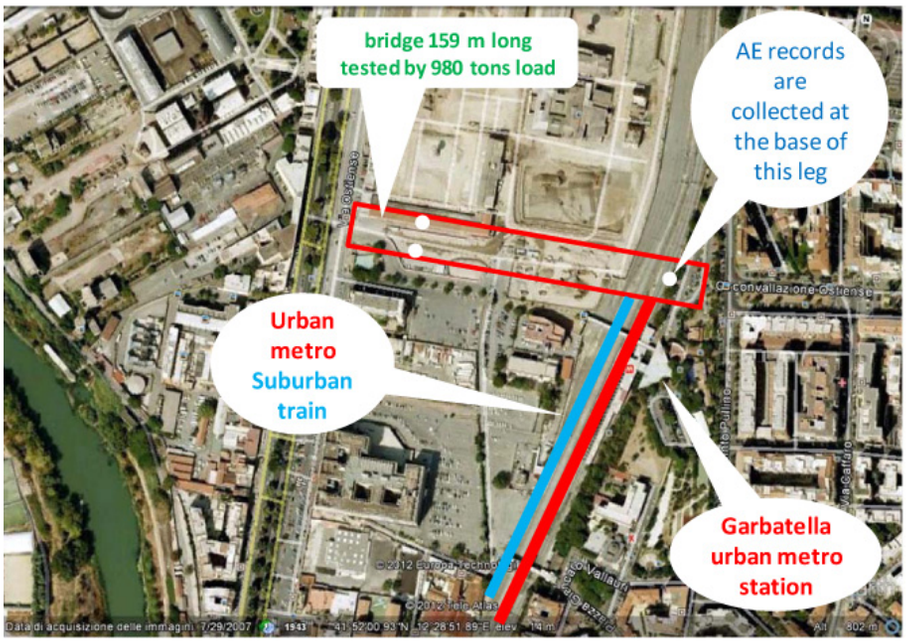

Figure 1. Sketch (out of scale), over a Google-Earth's image, showing the location of the Garbatella bridge. The urban metro line is indicated by a red strip, and the suburban train by a blue strip. The approximate locations of the three "legs" are indicated by white circles.

Figure 2. The Garbatella bridge seen from its western side. AE monitoring was carried out at the base of the single eastern "leg" here shown in the background.

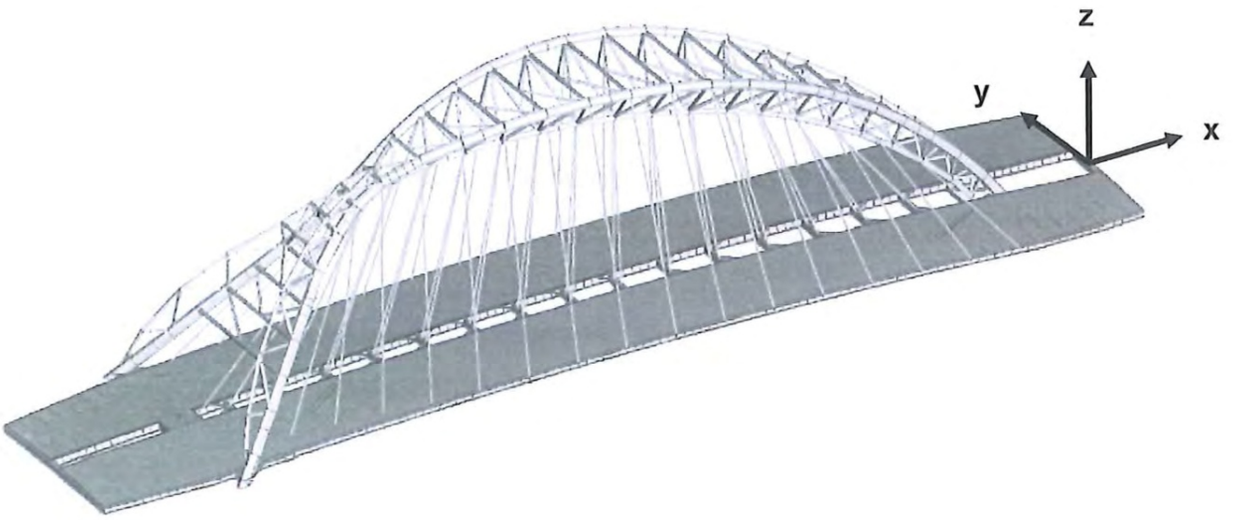

Figure 3. The *3*-leg spider cable-stayed Garbatella bridge. Its single eastern leg is to the right. Figure after the official documentation of the load test of the viaduct. See text.

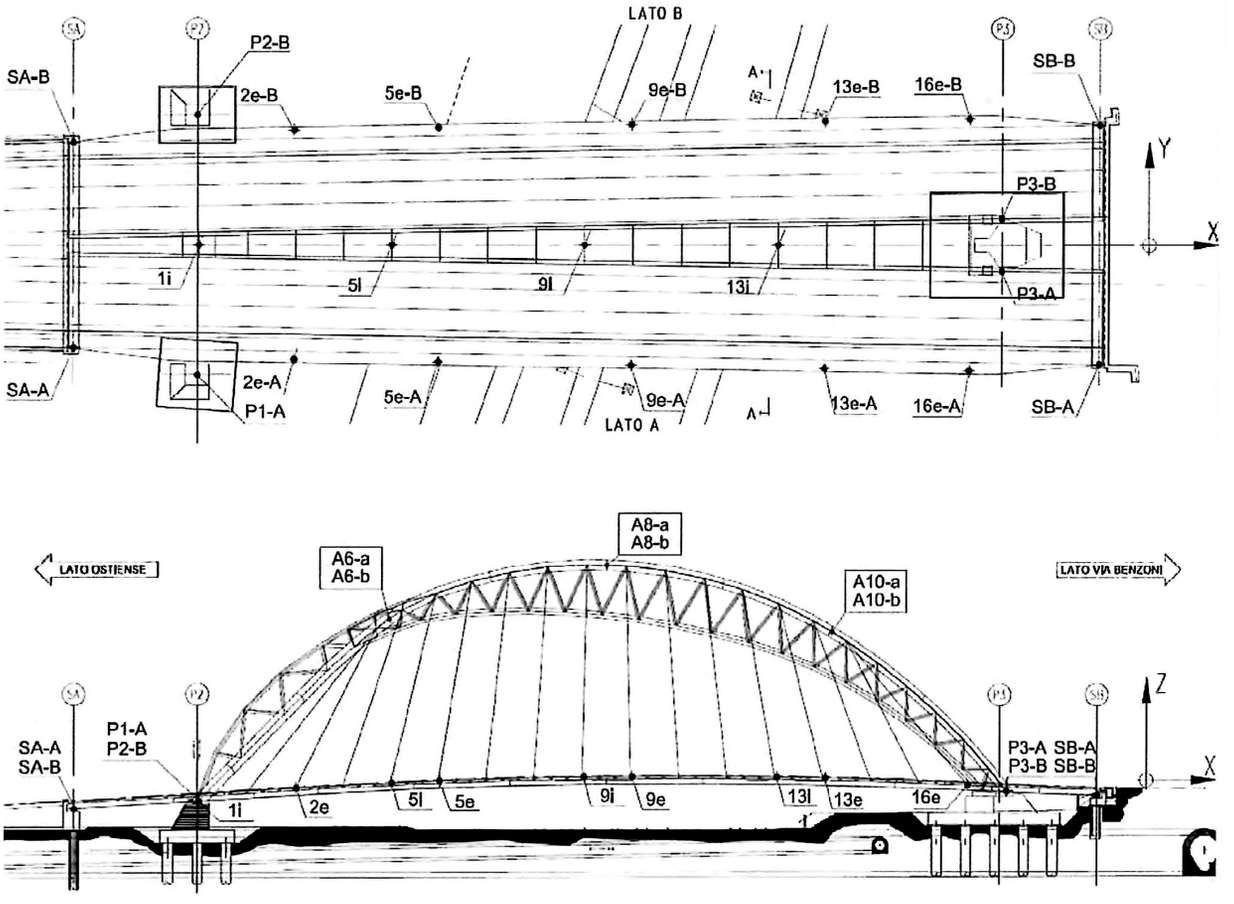

Figure 4. Horizontal and vertical orthogonal projection of the bridge. The eastern side is to the right. Figure after the official documentation of the load test of the viaduct. See text.

http://dx.doi.org/10.5772/54840

Only the details of *Step 1* are here of concern. The vertical displacement of the key of arch (side A) was measured as *-37 mm*, which resulted *92%* the model estimate *-40 mm*. The vertical displacement of the middle point of the road level (side A) was *59 mm*, which equals 95% the computed *62 mm*. The variation of compressive stress at the middle key of the arch (side A) resulted *-3930 kN*, which is *93%* the model estimate *-4243 kN*. The external suspension cable *9e* (side A) experienced a traction of *170 kN*, which is *97%* the estimated *175 kN*. A lower oblique chain under the road level, which opposes the longitudinal and lateral extension of the arch, experienced a traction of *3160 kN*, which is *89%* the estimated *3560 kN*. The sliding of the two western legs was (Δx, Δy, Δz, respectively, in *mm*): for the southern leg *(-11,-1,0)*, to be compared with model computation *(-12,-1,0)*, and for the northern leg *(-11,0,0)*, to be compared with model computation *(-12,1,0).*

Similar results, which however are not here reported in detail, were found concerning *Steps 2, 3* and *4* of the load test. The absolute values of all measured parameters resulted less than the estimated applied stress. They claim that this discrepancy derived from the size of the nodes of the arch, which in model computation were assumed point-like. Therefore, the model underestimated the true rigidity of the structure.

In general, the discrepancy between model and records resulted less than a few percent, which was explained by thermal dilation effects, originated by changes of air temperature. Owing to abrupt rain and hail, at the end of *Step 1* an air temperature variation had occurred ΔT = *-4°C* which affected only the arch of the bridge, but not its road level, as it was protected by road cover. According to model computation, it was estimated that this effect implies a lowering to the road level by *4 mm*. The discrepancy, *4 hour* later, when the absolute value of ΔT had diminished, was only *2 mm*. This result is consistent with the leading role of the thermoelastic stress, in agreement with what is clearly envisaged by the present investigation.

For future reference, the detailed load timing is here needed only concerning *Step 1*. Two trucks at a time were loaded, starting at $08^{h}\ 07^{min}$ *a.m.* (LT=UT+1 hour), attaining full load at $08^{h}\ 45^{min}\ 45^{sec}$. The loading occurred by adding *3* sets of mixers at a time. The first set, here called "load-1" set, involved *7* couples of trucks loaded during *9 min* (approximately at $08^{h}\ 07^{min}$, $08^{h}\ 08^{min}$, $08^{h}\ 10^{min}\ 45^{sec}$, $08^{h}\ 12^{min}$, $08^{h}\ 13^{min}$, $08^{h}\ 15^{min}$, $08^{h}\ 16^{min}$ LT). Then, *2* couples of trucks were loaded after a while (approximately at $08^{h}\ 24^{min}$ and $08h\ 34^{min}\ 15^{sec}$); this is here denoted as "load-2" set. The remaining *6* couples of trucks were loaded during *5.5 min* (approximately at $08^{h}\ 42^{min}$, $08^{h}\ 43^{min}$, $08^{h}\ 43^{min}\ 30^{sec}$, $08^{h}\ 45^{min}$, $08^{h}\ 45^{min}\ 45^{sec}$), and this is here denoted as "load-3" set.

The load test further continued through *Steps 2*, *3* and *4*. But, their detailed timing is not of interest for the present study. The entire load test was completed by late afternoon.

2. AE monitoring

AE were recorded (figure 5) at the base of the single eastern "leg", in two frequency bands: high frequency (HF AE) at *200 kHz* and low frequency (LF AE) at *25 kHz*.

Figure 5. The AE recording apparatus while it is implemented (upper figure), and details of the AE detector (lower figure), where every AE transducer is located inside a transparent plastic cylinder (left figure), and the two preamplifiers are the small white cylinders (right figure).

http://dx.doi.org/10.5772/54840

Per each frequency, the primary signal was released by a piezoelectric acoustic transducer. The signal was then pre-amplified and amplified. The rms amplitude of the signal was averaged over *5 msec*. The entire set of all these [*5 msec*]-averaged signals was averaged over a pre-chosen time interval Δt. Then, a data logger stored this final average over Δt into two distinct data series, for HF AE and LF AE, respectively.

The main time series of records lasted between *Dec* 16^{th} 20^{h} 58^{min} 59^{sec} through *Dec* 29^{th} 14^{h} 17^{min} 35^{sec}. Data were collected at Δt*=4 sec* and these series are here briefly denoted as the "*4s*" data set. It is almost uninterrupted, apart a few minor gaps. During one of these gaps, between *Dec* 20^{th} 12^{h} 14^{min} 58^{sec} through *Dec* 20^{th} 13^{h} 39^{min} 11^{sec}, data were recorded with Δt*=1 sec* and these series are here briefly denoted as "*1s*" set.

Meteorological conditions were substantially perturbed, with occasional relevant wind gusts, and episodic rain or hail precipitation. However, no anemometer was available, and no regular temperature record.

3. Data analysis: Algorithms and physical principle

Data handling was carried out by a set of a few different algorithms. Reference is made to previous literature[6]. Several applications of these methods already appeared in previous papers by the authors and co-workers, mainly concerned with the natural environment (crustal stress and volcanic precursors), but including also a few studies dealing with laboratory test, either on steel or on (non-reinforced) concrete.

The present paper is specifically focused on the output of a few algorithms, which are better suited to characterize the *overall* performance of the steel structure. Additional algorithms are to be later considered by additional investigations (in preparation), to be more specifically concerned with detailed features of the time-history of the response by the microcrystalline solid structure to the applied stress, both during load-time and during after-load recovery.

The identical data handling and analysis has been separately applied to both HF AE and LF AE series.

One key algorithm, here applied and briefly summarized, deals with the fractal dimension D_t of the time series of the AE records.

But a preliminary needed step is the *outlier rejection* which is applied to every AE raw data series. The purpose is to get rid of every AE signal that, owing to any physical reason (maybe sometimes even by unpredictable instrumental bad functioning but also by any other unwanted physical disturbance), eventually appears to deviate by a relevant amount with respect

6 As far as the methods are concerned, refer to Paparo et al. (2002, 2006), Gregori et al. (2002, 2005, 2007, 2012), Paparo and Gregori (2003), Gregori and Paparo (2004), and Poscolieri et al.(2006, 2006a), where several applications are discussed in detail. Other applications are here mentioned passim. Additional references dealing with applications and which are not mentioned in the following are: for laboratory experiments on concrete see Guarniere (2003) and Gregori and Paparo (2006); for Vesuvius see Paparoet al. (2004, 2004a); for Cephallonia Island see Lagios et al. (2004), and Poscolieri et al. (2006); and for fractal analysis on the geographical distribution of faults see Cello (2000) and Gregori et al. (2010).

to some "smooth" trend of its background. However, while dealing with every previous analogous AE investigation, the outlier series resulted *not* to be concerned with spurious and unwanted disturbances. Rather, it reflected an intrinsic physical feature, derived from the intimate physics of the microcrystalline structure of materials (see section 4). This same conclusion is also found in the present study.

The subsequent investigation of the outlier series, which is here reported, is then carried out by the algorithm "*arp*", which in the present application resulted particularly suited for the detection of some (maybe unexpected) oscillations of the bridge.

The algorithm for outlier rejection relies on some mathematical technicalities, which are not of specific interest for the present discussion. Therefore, owing to brevity purposes, they are not here explained. The interested reader may refer to the aforementioned literature.

Call $f(t)$ the data series of the records (of either HF AE or LF AE). It is a discrete set of values. In general, all values refer to successive time instants defined by a time increment Δt. According to the requirements by our algorithm, however, this regularity is only optional. For the *1s* set it is $\Delta t = 1$ *sec*, and for the *4s* set it is $\Delta t = 4$ *sec*. Reject the outliers.

Call $\bar{f}(t)$ a (weighted) running mean, computed only by means of the *non-rejected* $f(t)$. In the present analysis, a triangular weight-function was chosen with half-time interval ± 100 *sec*. This interval, however, may be arbitrarily changed inside comparatively loose constraints, and this choice results to imply only a physically insignificant consequence on results.

Call $g(t) = f(t) - \bar{f}(t)$ the residual, computed by means of all $f(t)$, i.e. *including* also the formerly rejected outliers.

Define a point-like process[7] identified with the time series of "AE events" defined as follows.

An "AE event" is identified with *one relative maximum* of $g(t)$. But the amplitude of this relative maximum must to be above some arbitrarily pre-defined *threshold*, defined as follows.

Consider a reasonably wide subset of the original series of $g(t)$. Call "*S*" this subset. Compute the rms value σ of all $g(t)$ contained in "*S*". In the present case, the aforementioned threshold has been chosen as $[\sigma/4]$ for the reasons explained below.

Choose another arbitrary and suitable time interval Δt_1, which is used to evaluate D_t. For every given pre-chosen time instant t_j (for *j=1, 2,...*), consider the set "*M*" of all elements of the aforementioned point-like process, which occur inside a moving time lag of total duration Δt_1 and centred at the given t_j. Apply the box counting method,[8] and compute the fractal dimension $D_t(t_j)$ (for *j=1, 2,...*) of the set "*M*". This $D_t(t_j)$ is one leading parameter in the present discussion.

7 A "point-like process" is the conventional name used in mathematics to denote a time series of "yes" events (e.g. a heartbeat, a natural catastrophe, an earthquake of magnitude larger than a given threshold, a volcanic eruption, a flood, etc.). Every event is characterized by its abscissa (i.e. time in the present case history), independent of its ordinate (or intensity).

8 This is a well known algorithm and its description may be easily found on every elementary textbook on fractal analysis.

http://dx.doi.org/10.5772/54840

The criterion used for the definition of the aforementioned *threshold* began by choosing ten trial values for the threshold, everyone arbitrarily defined as [σ/k] (with $k=1, 2,..., 10$). The fractal dimension D_t(k) was computed on the entire aforementioned subset "*S*", and for every given k.

Owing to physical reasons, if k is exceedingly large, a threshold chosen equal to [σ/k] results exceedingly small. The background noise is thus included and some false "AE events" enter into subsequent computation: owing to its mathematical definition, a large D_t(k)~1 must therefore be found.

In contrast, if k is exceedingly small, [σ/k] results exceedingly large, and the threshold excludes several physically significant "AE events", which are erroneously likened to background.

Therefore, owing to mathematical reasons, the plot of D_t(k) *vs.* k certainly is monotonic and decreasing. But, whenever a step-like decrease is observed on this plot, this denotes the correct k value, which excludes the entire background noise, while it keeps all values which are physically significant. Hence, this k defines the correct logical ''sieve'' that rejects noise and saves the physical significant information. The optimum choice was thus found to be $k=4$.

However, in the present data analysis - and concerning both *1s* and *4s* sets - it is convenient to consider the definition of Δt_1 from a different viewpoint. Let us refer to the *order number* of the elements of the point-like process, rather than to their respective *time instant*. In the present application, this makes no difference, as the original AE data series was recorded at constant time increments Δt.

Three choices have been made for each *1s* or *4s* set. Every single $D_t(t_j)$ was computed by means of N_D elements, which are included in the aforementioned Δt_1 moving time lag. It was chosen either $N_D = 600$, or $N_D = 1200$, or $N_D = 1800$ elements. In the case of the *1s* data series, this implies that the evaluation of every $D_t(t_j)$ was carried out by referring to running time intervals of total duration *10 min*, *20 min*, and *30 min*, respectively. In the case of the *4s* data series, this corresponded to evaluate a $D_t(t_j)$ by referring to time intervals of *40 min*, *80 min*, and *2 hours*, respectively.

These different choices of N_D were considered, because a different N_D eventually plays a relevant role when dealing with the error-bar and scatter of the time series of computed $D_t(t_j)$ *(j=1, 2,...)*. The reason is the unknown response to unwanted disturbances, originated by several physical environmental perturbations (see section 5). This N_D choice resulted comparably critical for HF AE, while concerning LF AE series it appeared robust.

As already mentioned, other algorithms for data analysis are to be considered (in preparation), which are more directly focused on details of the response of the microcrystalline steel structure. But, as far as the present analysis is concerned, only one relevant physical item ought to be here anticipated.

According to the so-called "hammer effect" (see Gregori *et al.*, 2007), we found that, in the present AE records, the AE release almost always occurs *only* during the "recovery stage", rather than during the "hammer stage". That is, no AE release occurs while the material is subjected, on an instant basis, to an externally applied stress. Rather, the AE release occurs as

soon as the micro-crystals recover during their (approximately) "elastic" response, after the former applied stress. But, owing to brevity purposes, no additional details can be here given.

Another algorithm used for the present study is the "*arp*" histogram[9] applied to both outliers time series. This algorithm may be applied to every point-like process. Every event is considered independent of its intensity, and only the time instant of its occurrence is considered. Call $\{t_j\}$ $(j=1, 2,...)$ the time series of a point-like process, and call $\Delta t_{j,k}$ $(j,k= 1, 2,....; k>j)$ the set of *all* possible time intervals between the time instants of *any* couple of successive (even non-contiguous in time) elements of the set $\{t_j\}$.

"*Arp*" is the histogram of these $\Delta t_{j,k}$ $(j,k= 1, 2,....; k>j)$. But, it is well known that a histogram can be drawn only after choosing a suitable elementary time increment Δt_e on abscissas, such that all the elements that occur during every given time interval Δt_e of the histogram are supposed to be associated with an identical occurrence instant of time. Practically, it resulted convenient to define Δt_e equal to $(1/10)$ the average of all $\Delta t_{j,k}$ $(j,k= 1, 2,....; k>j)$.

As it can be easily shown (just try it), owing to definition, if the point-like process is a random series, its "*arp*" must look like a rectangular triangle, with a regularly decreasing trend. In contrast, if the system has some leading component characterized by a periodicity T_0, its "*arp*" will display approximately the same roughly decreasing trend, and a scatter superposed on it with relative maxima at every abscissa hT_0 $(h=1,2,...)$.

Denote by T any general value for an abscissa of "*arp*" abscissas and call $n(T)$ its ordinate. The error bar of "*arp*" is expressed as $n(T) \pm \sqrt{n(T)}$. Since this error bar depends on $n(T)$, the assessment may eventually result ambiguous of the occurrence of a relative maximum of $n(T)$. This drawback can, however, be easily avoided by considering the histogram defined by $\sqrt{n(T)} \pm 1/2$, which has a constant error bar, and will be here briefly denoted as $\sqrt{arp}$.

In the next section a concise summary is given of the primary physical principle. This is the basis for entire physical rationale of all previous algorithms. Section 5 deals with the analysis of D_t and with the way to recognize and rebut unwanted environmental disturbances. Section 6 deals with the "*arp*" (or $\sqrt{arp}$) analysis of each outlier series.

4. The physical rationale

No material exists that is either ideally "elastic", or ideally "plastic". Every time that every real approximately "elastic" and solid medium experiences a stress, it also experiences a fatigue. For instance, even a tenuous thermal deformation is a cause of ageing of the medium.

The fatigue, or ageing, of the material is manifested as a rupture of some crystalline bond. Whenever an additional stress is applied, new bonds yield. But, in general, these new ruptures occur close to formerly broken bonds, where the crystalline structure is comparatively weaker.

9 "Arp" is an acronym for "automatic research of periodicities". "Arpa" is the Italian name for harp.

http://dx.doi.org/10.5772/54840

In this way, a true chain-reaction occurs. This is the physical explanation of the well known phenomenon of cleavage plane in a crystal.

Every time that a crystalline bond yields, some AE is released, which is propagated through the medium. The primary physical information of our method relies on the timing of the sequence of subsequent AE release, which is detected inside the medium.

It should be pointed out that the concern is not about the intensity of the AE signal. There is only need to assume that the signal has a sufficient intensity in order that it can be detected. Indeed, the recorded AE amplitude is controlled by several unknown factors, such as by the distance and intensity of the instant AE source, but also by the unknown and eventually time-varying damping of the signal between source and detector, etc.

In contrast, the *timing* of the detected AE signal results to be an information of paramount importance in order to check how the medium responds to an applied stress. In this way, the ageing of the medium can be effectively monitored, and its eventual loss of performance. The entire procedure is therefore purely passive, and no invasive action is required.

An important related concept deals with the *frequency* of the AE signal, which depends on the size of the micro-flaw, which is associated with the broken bonds: comparatively smaller flaws release comparatively higher frequencies. We cannot know the law that relates flaw size and AE frequency, but we do know that this is the physically correct rationale.

While the ageing process is in progress, small flaws coalesce into larger ones. A former population of comparatively smaller flaws thus progressively decays, while it generates an increasing population of larger flaws etc.

Define "flaw domain" (Gregori *et al.*, 2012) the typical physical domain of a flaw, which is associated with the observed AE of a given frequency (although we do not know the real size of this flaw domain). The statistics of flaw domains for a given AE frequency shall display a lognormal distribution.

This inference derives by consideration of the rationale of the simplest case history of the so-called Kapteyn class distributions (Kapteyn, 1903, 1912; Katpeyn and van Uven, 1916; Paparo and Gregori, 2003). That is, the probability of occurrence of an event is proportional to the number of identical events that are occurring at the same instant of time. For details and reference see the aforementioned literature. Owing to definition, a lognormal distribution is asymmetric. It has a tail, and this can be promptly shown to be the primary physical cause for the aforementioned persistence of outliers, both in $f(t)$ and in $g(t)$, independent of the "sieve".

We know therefore that one and the same kind of anomalous behaviour is to be expected to be observed first by AE of comparatively higher frequency, and subsequently by AE of every progressively lower frequency, etc. This is of paramount important, as it provides us with a *physical* information on the *direction of the time arrow* inside the ageing process. That is, we can thus recognize a *precursor* phenomenon compared to an *after-event* occurrence. For instance, in the case of seismic precursors, or of any kind of other environmental measurements, the practically unsolvable problem is well known of the assessment, on a statistical basis, of what is a *precursor* compared to what is an *aftershock*.

Summarizing, it is possible to monitor the ageing of a material - and the loss of performance of a structure (either natural or manmade) - simply by a passive monitoring of the AE released by its medium, when it responds even to a very gentle stress.

When an AE experiment is carried out in the laboratory, we can very effectively control the physical system, and by this we can minimize the impact of unwanted disturbances. In contrast, when operating in the field, this is impossible, and it is therefore important to record environmental perturbations in order to assess their respective impact on the AE records and on their interpretation.

While exploiting the AE monitoring of the Garbatella bridge, unfortunately no regular meteorological records were available. Hence, the meteorological disturbances had to be assessed by means of an *a posteriori* analysis on both AE data series.

In this respect it has to be pointed out that we deal with D_t which is treated like a *performance index*. Its temporal trend is considered and, on its basis, an eventual alert is to be issued according to some pre-defined and well assessed protocol.

But, in general, while evaluating the D_t *vs. t* trend, two distinct operative case histories are thus to be envisaged.

- In one case, every AE event primarily responds to one applied stress impulse, which is originated by an external action applied to the system. For instance, consider the case history of a volcano. Its endogenous hot fluids eventually repeatedly and progressively increase their pressure. The pores of the medium of the volcanic edifice experience an ever increasing number of yielding of flaw domains. As long as the solid structure of the medium affords to sustain the increasing pressure, it is found that D_t remains reasonably small. But, when the pressure increases, also D_t shall increase, as an ever increasing number of flaw domains will randomly yield per unit time. When D_t increases until reaching *1* the volcanic edifice shall unavoidably yield, and a new boca is opened. This time sequence was observed e.g. on the occasion of the recent Stromboli paroxysm (Gregori and Paparo, 2006).
- The second case history is to be considered when the externally applied stress is only a trigger, and we observe only the subsequent evolution of the medium, while it searches for a new equilibrium state, after having suffered by the previously applied stress. In this case, a "young" medium first responds with a D_t close to *1*, because the ruptures of its bonds occur randomly, as no previously organized flaw domains exist inside it. In contrast, an "aged" medium will display a progressively decreasing D_t and the lower is D_t the more "aged" is the medium.

For instance, while carrying out experiments on some steel bars (Biancolini *et al.*, 2006), it was found that when $D_t \sim 0.45\text{-}0.5$ the bar is very close to break (different steels ought, however, to be tested in the laboratory, in order to assess an eventually different security threshold for different alloys).

Differently stated, D_t denotes how far every AE event keeps a memory of other AE events either that occurred before it, or that are going to occur after it. No memory exists in a random sequence of AE event, the medium is therefore "young", and it is found D_t =1, just due to the

http://dx.doi.org/10.5772/54840

mathematical definition of randomness. When the medium suffers by progressive ageing, its flaw domains get progressively organized towards the final organization of a cleavage plane. This entire process is illustrated and quantitatively measured by the time evolution of D_t towards progressively lower values.

5. Steel ageing — The D_t analysis, and the rejection of environmental disturbances

Concerning the AE monitoring of the Garbatella bridge, for clarity and brevity purposes let us anticipate a few much general inferences and conclusions.

A higher temporal resolution ought to be recommended. An AE datum ought to be recorded, at least, every *50-100 msec* (rather than every *1 sec* or every *4 sec*).

Consider the warning of section 4. When the external trigger caused by an environmental agent is repetitive, displaying some peculiar time sequence, the resulting AE signal - when it is interpreted according to the present rationale - may eventually simulate a false effect. Therefore, while one operates in the field, a sum of unknown and unpredictable disturbances must always be suitably taken into account, and whenever needed rejected.

This drawback is found to be particularly severe for HF AE, which are much more directly related to the primary external input. In contrast, owing to physical reasons (see section 4), the LF AE are more directly related to the downgrading of the crystalline structure. Indeed, LF AE are released when the material has already evolved and some conspicuous amount of comparatively large flaw domains have already been generated. Therefore, LF AE are to be expected to be much more indicative of the real loss of performance of a structure, while HF AE ought to be much better representative of the diachronic history of its external disturbances.

In terms of an expressive analogy, it is like listening music while a child close to you abruptly and loudly cries. The child noise has to be rebutted in order to appreciate the music in the background. Similarly, the ageing of the structures can be appreciated only after rejecting unwanted, even "loud", disturbances.

Summarizing, the primary scope of the analysis of a data series measured in the field is the distinction between the effects associated with the unknown timing of some external input, compared to the time history of the AE release determined by the evolution of the ageing process inside the medium which is to be monitored. In addition, the "perturbation" by external causes, which may eventually simulate a false behavior, is much better evidenced by means of HF AE compared to LF AE.[10]

One additional relevant concern, related to the role of the external trigger, deals with a technological problem, i.e. with the time required by the whole AE recording device to reach

10 This conclusion is evident from the "macro-analysis" which is here presented. But it is also confirmed by a much more detailed - "micro" rather than "macro" – analysis, which is the object of a different investigation (in preparation).

its operative regime. During a limited initial time-lag, a sum of several normally unknown factors apparently perturb the AE records. This lag has to be empirically determined, mostly whenever one wants to carry out once in a while a rapid test of performance of a given structure (the purpose is to avoid, sometimes and whenever possible, a steady AE monitoring, which is comparatively more expensive and time consuming).

Summarizing, we have to distinguish (mainly for HF AE but also in LF AE) between AE signals caused by an accidental trigger compared to the AE signals which are passively released by the material and are specifically suited to monitor its ageing.

It is therefore here first shown how we first assessed the role of a few typical and relevant disturbances. The Garbatella bridge is "young" and performing. The target of the present test-experiment is therefore to calibrate the procedure of AE analysis, in order to check and assess a general procedure suited to investigate the performance of every old bridge.

We thus realized that - compared to the time of its formal load test - the viaduct suffered by a comparatively greater stress during the previous day, when the road cover was laid down.

Figure 6 is a plot of the raw signal for both HF AE and LF AE *4s* sets, while the *1s* set is discussed only here below, when dealing with a specific item (see figure 22). An exponential decay trend is superposed on either plot to represent the recovery of the bridge after the stress that was applied during *Dec 16*th and *17*th. The HF AE time-constant of the decay is about half the time-constant for LF AE, consistently with the fact that HF AE, compared to LF AE, are more directly associated with a shorter-lived effect.

For future reference, it should be pointed out that the HF AE signal is very low, almost null (although not strictly null; see below) except during the warmer hours of the day (say between noon and 5 p.m.). This denotes that the signal amplification was insufficient in order to detect the AE signal other than when the thermoelastic deformation was conspicuous. This is a typical case history that shows that the instrumental amplification of the original AE signal was suitable only during some hours of the day, while during other hours the recording system was in underflow.

The most important inference which deals with material ageing is represented by $D_t(t_j)$ computed for LF AE and by the *4s* data set (figure 7). The three different computations, by N_D=*600*, or N_D=*1200*, or N_D=*1800* for every $D_t(t_j)$ computation, result remarkably similar.

Every apparently much dramatic very low value for $D_t(t_j)$ is the expected response to every sporadic disturbance originated by finishing works in progress on the viaduct. The viaduct was not open to public, and a conspicuous amount of finishing activity was in progress during the *~ 13 days* spanned by the *4s* set. Drills were occasionally used, operated inside either the metal components or the concrete basement of the "legs". Since the bridge is a very efficient AE probe, composed of a monolithic body with an excellent conduction of ultrasounds, the action of a drill - or of any kind of strong friction which causes some relevant local destruction of crystalline bons – must produce an LF AE signal with some very low $D_t(t_j)$. This is the same effect as the aforementioned "loud" disturbance by the cry of a child while you listen music.

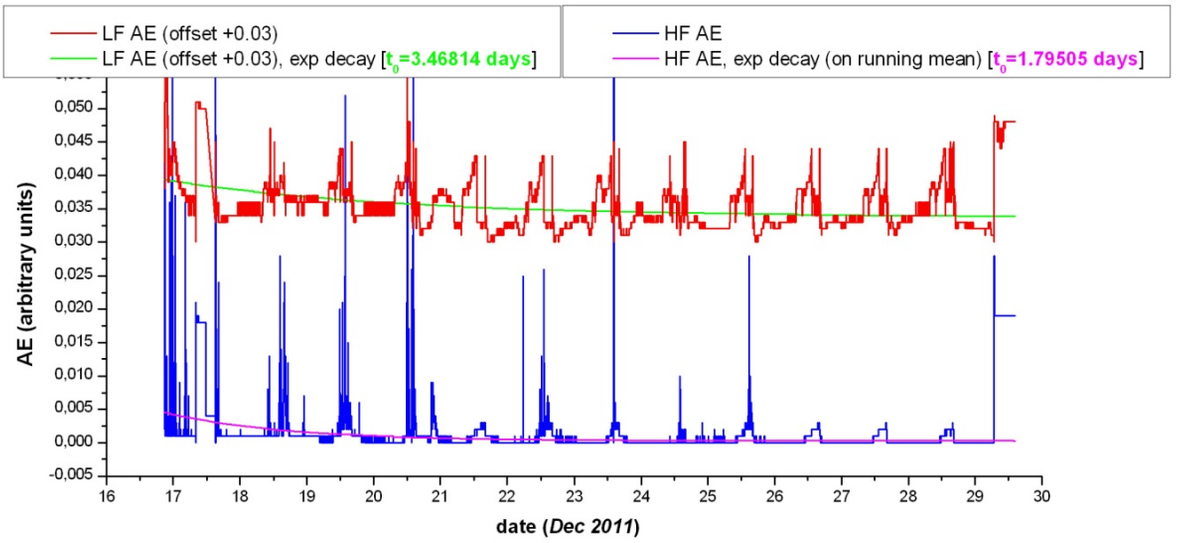

Figure 6. Raw data of the *4s* data sets. The cause is unknown of the abrupt upward discontinuity at time instant *29,28337* (it was probably instrumental while disassembling the AE recording device). An overall interpolated exponential decay is superposed (computed on $\tilde{f}(t)$ for LF AE and on $f(t)$ for HF AE and by excluding the unreliable final discontinuity). The time constant is *1.795 ± 0.016 days* for HF AE and *3.468 ± 0.043 days* for LF AE. That is, the recovery of steel after load-test is about twice more rapid for HF AE compared to LF AE flaw domains. Note that the detected HF AE signal is significant only during the warmer hours of the day, while during the remaining hours in general the AE detecting system is in underflow. See text.

Another cause of much dramatic very low value for $D_t(t_j)$ is the eventual underflow of the AE detection device. Indeed, if the recorded AE signal is e.g. constant in time (e.g. at its lowest sensitivity value, i.e. *1 mV* on the scale plotted in the figures here shown), it is found $D_t(t_j)=0$. This can be formally checked, but it also represents the fact that, when all AE records are identical, the physical system has a complete memory of all AE records which occur at every other instant of time.

Note that all these features are evident independent of N_D. The algorithm is robust. The real relevant information about the ageing of the metal components of the viaduct is therefore represented by the long-range trend of the average value of $D_t(t_j)$, which is found to be intuitively close to $D_t \sim 0.8$.

The analogous D_t time series for HF AE, shown in figure 8, denotes a comparably less robust response to the N_D choice, but no clear inference. When the AE recording system is underflow (see figure 6) no D_t can be computed, according to the argument mentioned here above. Figure 8 displays therefore an approximately diurnal periodical trend, because the system detects AE signals, with a significant time-varying intensity, only during the warmer hours of the day.

Therefore, we smoothed the $D_t(t_j)$ data series by means of a weighted running average, with triangular weight over *6 min 40 sec*. The result for HF AE is shown in figure 9, which displays three time intervals with comparably much different trend. The initial and final time intervals appear to be steadily increasing. At present, it has been impossible to envisage the physical reason of this behaviour. Environmental disturbances ought to be monitored, dealing either

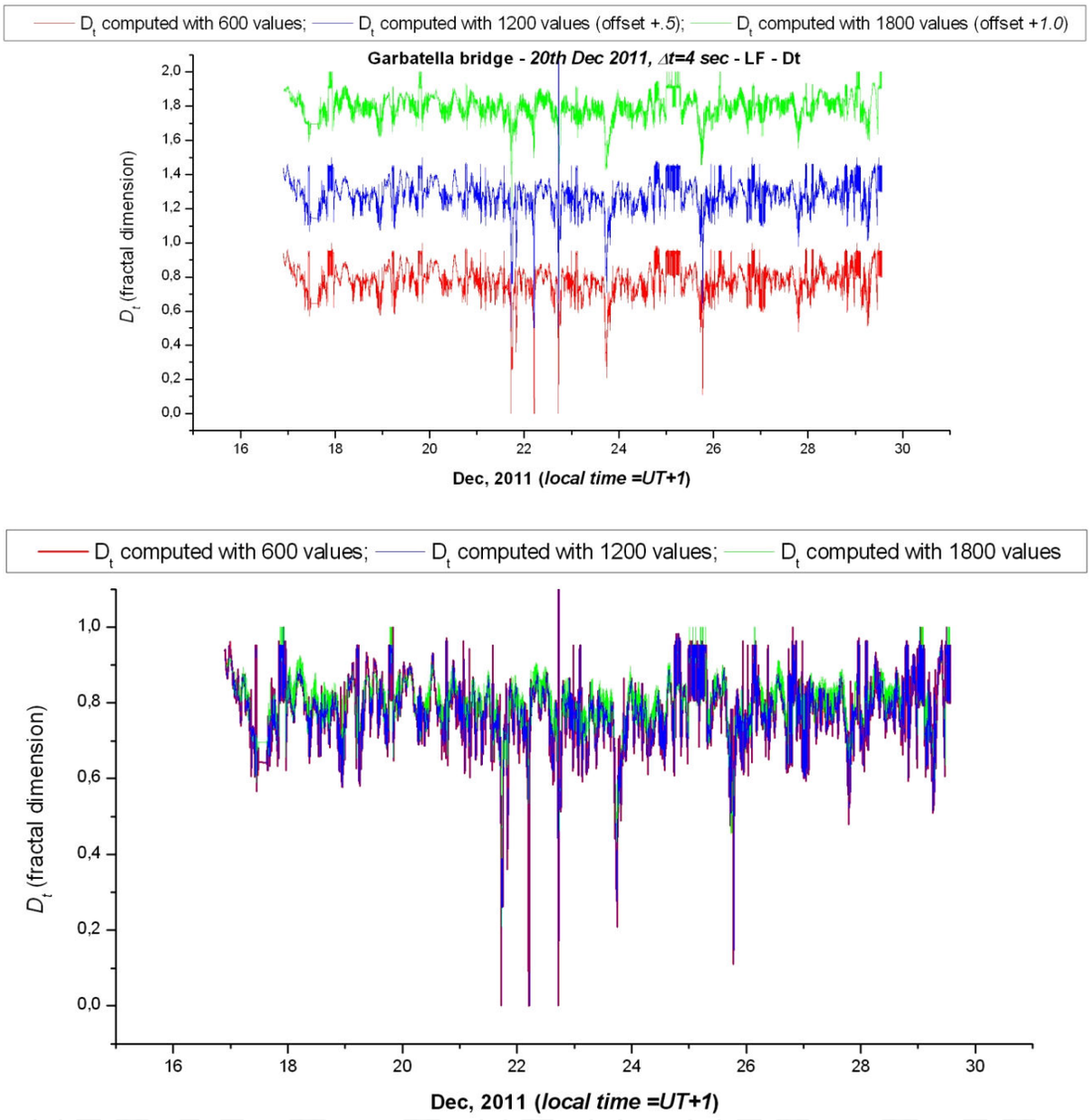

Figure 7. Fractal dimension $D_t(t_j)$ computed for LF AE of the *4s* data set, by using $N_D = 600$, or $N_D = 1200$, or $N_D = 1800$. The same values are plotted with offset (upper plot) or superposed (lower plot). The excellent performance of the viaduct is shown by the average trend at a steady $D_t(t_j) \sim 0.8$ value, while the scatter is caused by wind gusts and/or by the finishing activity that was in progress on the bridge and/or by underflow of the AE recording device. See text.

with meteorology or with manmade actions. In addition, long data series ought to be always recommended, in order to avoid boundary fringe-effects that, at least in principle, can never be fully avoided. In contrast, the intermediate time interval displays an exponential recovery, with a time constant *2.687 ± 0.066 days* which is of the same order of magnitude (*~1.8 days*) of the time constant displayed in figure 6.

http://dx.doi.org/10.5772/54840

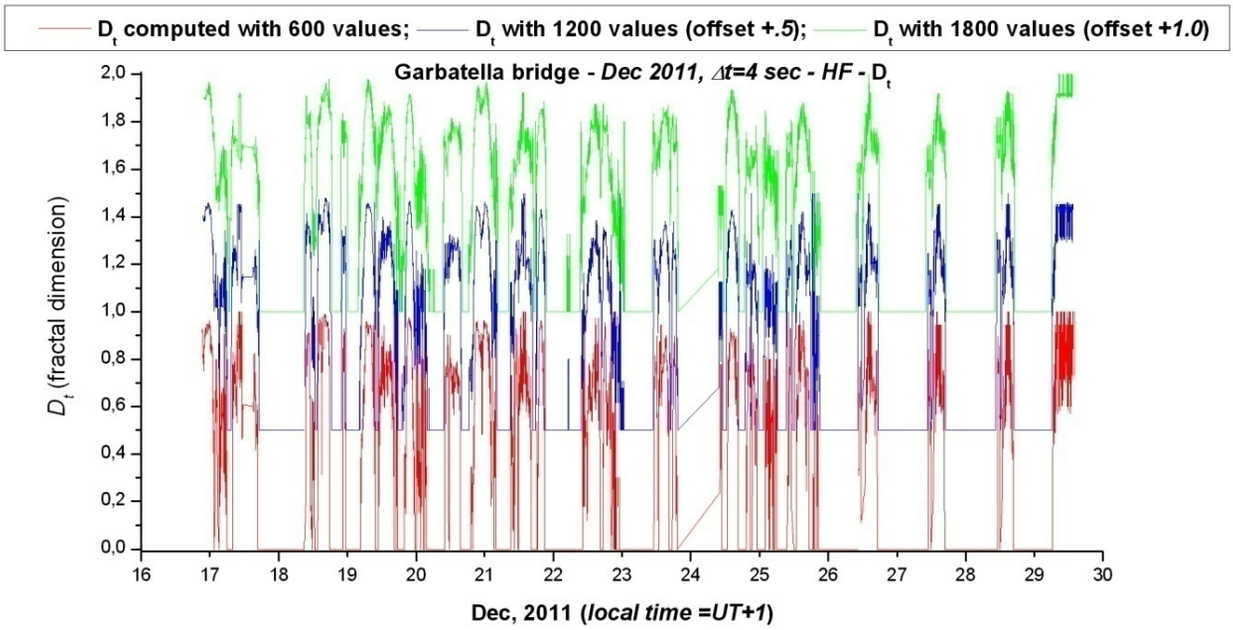

Figure 8. Fractal dimension $D_t(t_j)$ computed by HF AE of the *4s* data set. Only the plot with offset is shown. Compared to LF AE, this plot appears somewhat less robust with respect to the choice of N_D. When the AE recording system is underflow no D_t can be computed. Hence, this plot displays an apparent diurnal variation, because D_t can be computed only when AE records are available, i.e. only during the warmer hours of every day when a conspicuous thermoelastic effect was ongoing. See text.

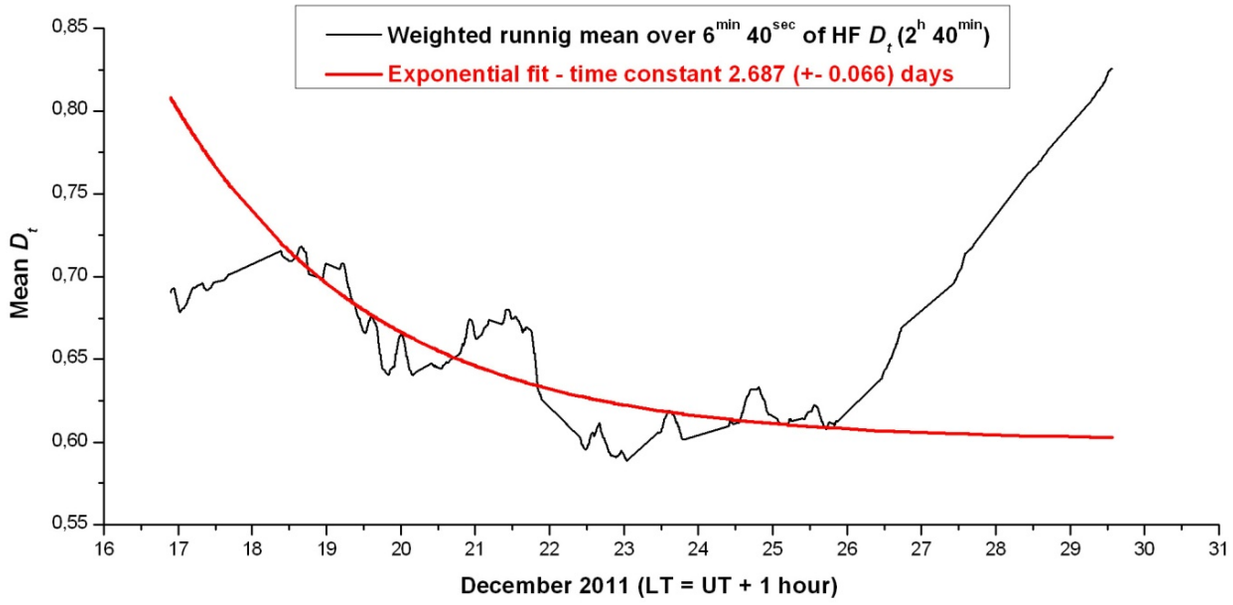

Figure 9. Weighted running average of $D_t(t_j)$ for HF AE by a triangular weight over ±3 *min 20 sec*. The initial and final steadily increasing trend is unexplained, and it is likely to be maybe associated to environmental disturbances or fringe effects. The exponential trend of the intermediate time lag displays a time constant *2.687 ± 0.066 days*, which is of the same order of magnitude of the time constant displayed in figure 6. See text.

The same procedure was applied to the LF AE data series. Figure 10 shows quite a different result. No regular exponential decay is anymore clearly detectable. Rather, the steel responds abruptly to every temporary time-varying externally applied stress. This is particularly evident on *Saturday Dec 24*th, *Sunday Dec 25*th, and *Monday Dec 26*th, because, owing to Christmas' holiday, basically no working activity was in progress on the bridge, which was rather subjected only to atmospheric disturbances.

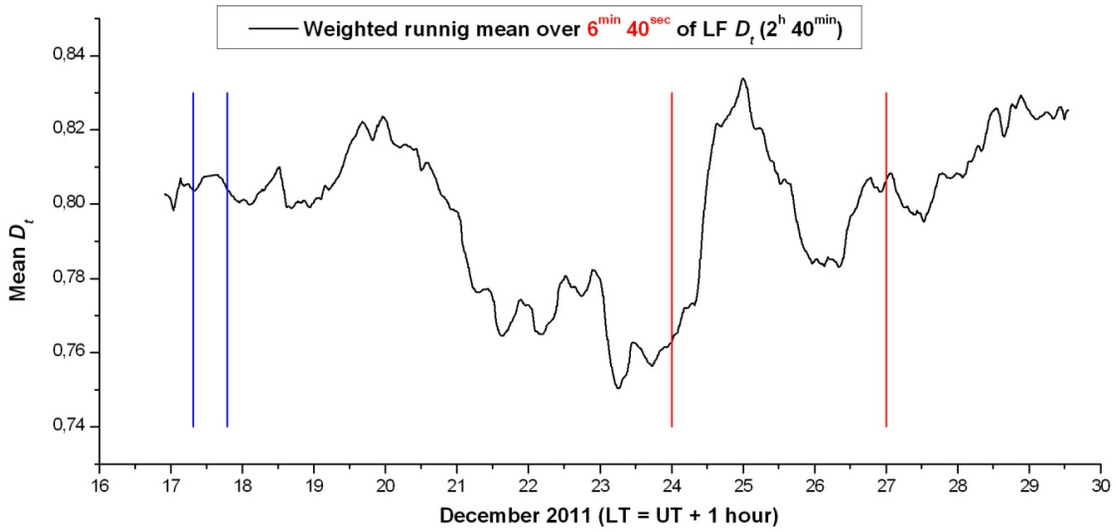

Figure 10. Weighted running average of $D_t(t_j)$ for LF AE by a triangular weight over 3 *min 20 sec*.. The load test on *Dec 17*th is evidenced by blue lines, and the holiday time on *Dec 24*th, *25*th, *26*th, by red lines. See text.

This means that HF AE, compared to LF AE, reflect a substantially much different feature of steel behaviour. HF AE reflect some much preliminary response, compared to LF AE which rather detect the substantial subsequent implications for crystalline structure, which are manifested as a later consequence of the primary applied external stress.

In any case, the prompt performance and reliability appears evident of this "young" viaduct, even during this much disturbed period of time, because the steel response denotes a rapid recovery after every applied stress, which promptly brings back the $D_t(t_j)$ value to a high and reliable level. Therefore, the medium is performing, even though the bridge, as a whole, has a slow recovery, as displayed in figure 6. In contrast, in the case of an older bridge, it is reasonable to expect that the steel ought to result much less performing, being denoted by a lower mean D_t trend.

In this respect, two laboratory tests ought to be recalled. A perfectly "young" material has an ideal abstract value $D_t(t_j)=1$. In contrast, its ageing is monitored by the relative decrease of $D_t(t_j)$. An experiment on some suspension blades of martensitic steel (Braccini *et al*., 2002) showed a progressive decrease from $D_t(t_j)\sim 1$ (when the blade was never bent after melting) to $D_t(t_j)\sim 0.6$ (after it had been bent only a few times). Then, the crystalline structure of the martensitic steel apparently attained its working regime. Thus, it finally displayed a steady performance.

http://dx.doi.org/10.5772/54840

Only after some heavy and repeatedly applied stress, a steel bar is to be expected to break. Experiments carried out on small steel bars (Biancolini *et al*., 2006) were pushed until final rupture of every specimen. It was thus found that that when it is $D_t(t_j) \sim 0.45 - 0.5$ the steel is almost close to total rupture. It should be stressed, however, that these alert values ought to be calibrated for every specific steel alloy.

Hence, it has to be expected that, in the future, the $D_t(t_j)$ of the Garbatella bridge ought to decrease until reaching a standard and steady working regime [maybe $D_t(t_j) \sim 0.6$ if the same threshold applies for the steel of the viaduct compared to the steel of the aforementioned laboratory experiment on martensitic blades]. This $D_t(t_j) \sim 0.6$ will characterize its performance during the largest part of its existence. In contrast an old bridge, with collapse hazard, ought to have already slowly approached its final alert threshold of $D_t(t_j)$. It should be always stressed, however, that this threshold has to be assessed, in every case history, upon considering the specific kind of steel by which it was constructed.

As far as the cause of the scatter is concerned of raw data and of $D_t(t_j)$, no anemometer records were available. Hence, the role of wind can be only indirectly investigated in the present study. During those days strong gusts of wind frequently occurred. According to the personal witness of the two co-authors (SP and GV) who set up and operated the instruments, on the occasion of every wind gust the recording device experienced strong transient perturbations, mostly in HF AE. Hence, they tuned the signal amplification on these wind gusts, and the HF AE recording device later resulted in underflow during calm periods, with low thermal excursion.

In any case, as far as the available AE data are concerned, several different specific kinds of disturbances can be distinguished and recognized as explained in the following subsections.

5.1. Thermoelasticity, and the effect of a time-varying load

Figure 11 is a superposed epoch representation of LF AE records of the *4s* set. The smoothed function $\bar{f}(t)$is superposed, instead of the raw data, in order to reduce scatter. A few physical facts are clearly evidenced, and a few days are indicated by a label on the figure.

During the entire *Dec 16*th heavy works were in progress on the viaduct, when a thick first layer of material was posed on the bridge for roadbed preparation. According to an indicative estimate, a *6 cm* layer of binder was laid down, with a total load of *~ 200 tons* on each 3-lane way. In addition, construction machines were used, which had a total weight of *~ 100 tons.*[11]

After *9 p.m*. of *Dec 16*th until *7 a.m*. of the *Dec 17*th, the bridge was recovering after its violent stress.

During *Dec 17*th (red line), at *~8 a.m*., the load-test was started, with dramatic consequences on the LF AE signal. Note that the straight line is associated with a period of time during which no records were available, due to a temporary failure of power supply.

11 We thank Ing. Francesco Del Tosto for providing us with this information.

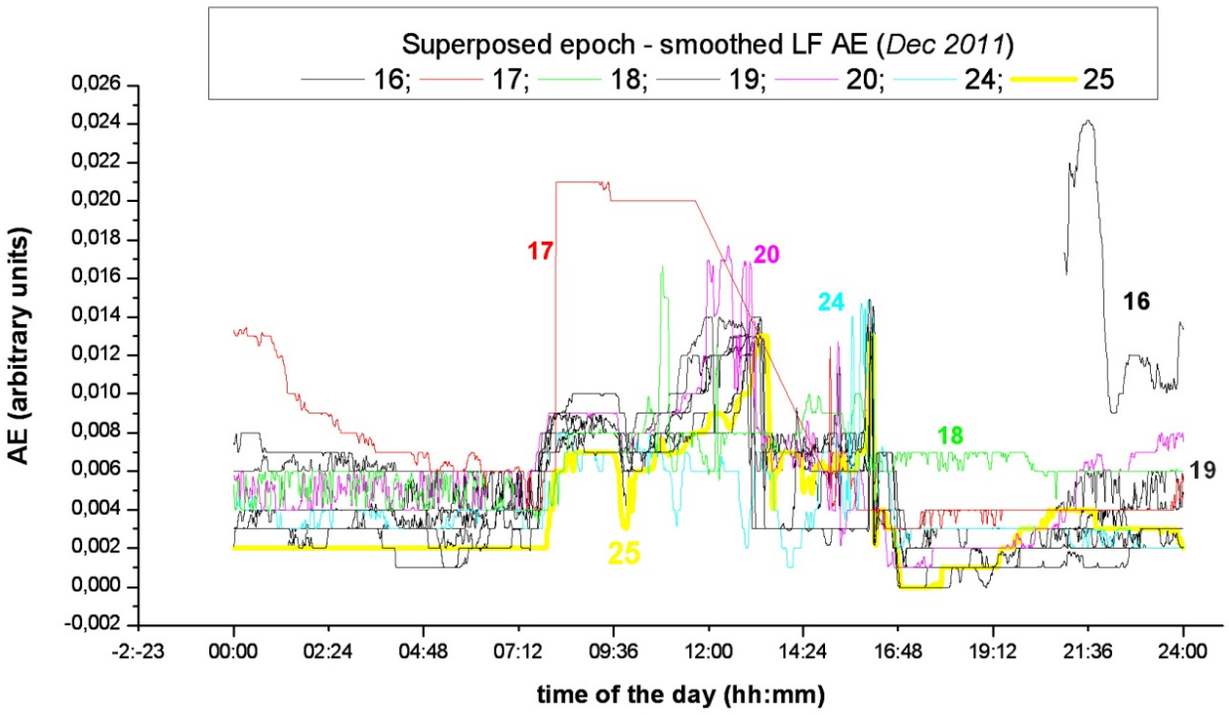

Figure 11. Superposed epoch representation (or "cycle diagram" for *24 hour* period) of the LF AE records of the *4s* set. The smoothed function $\bar{f}(t)$ is used instead of raw data in order to reduce the scatter. The labels on a few colored lines are the date (*Dec 2011*). No offset was applied. The difference between the lowest level of different days day depends on the relaxation process shown in figure 6. Note the dramatic behavior during the late *Dec 16*th and early *Dec 17*th consequent to the stress applied while laying down the roadbed. See text.

During the subsequent days, the most intense LF AE signal was recorded during working hours (say roughly between *8 a.m.* through *5 p.m.*), envisaging an effects associated with the stress applied while finishing the bridge.

But, it appears curious the fact that also on *Dec 25*th, Christmas Day, when no work was ongoing on the bridge (yellow line), some relevant LF AE signal was observed. In addition, in general, on every day a comparatively more intense signal was recorded almost at the same local time, i.e. during the early afternoon until ~ *4 p.m.* Therefore, this appears to be a likely thermoelastic effect.

In addition, in general a reasonably ordered and regular scatter was observed every day before *7 a.m.* (except on *Dec 17*th, when the bridge was recovering after the stress of the previous day). In contrast, the comparative trend on different days after *6 p.m.* appears more varied, maybe depending on different air temperature (for which, however, no record is available).

All these features are suggestive of a thermoelastic effect, which, in principle, ought to be expected to be manifested in two different ways.

On the one hand, a thermoelastic effect - which is certainly conspicuous on concrete or brick bridges - is similar to what is observed on the Gran Sasso mountain data series (a massif in central Apennines) by AE records measured in a deep cavern (Paparo *et al.*, 2002; Gregori and

http://dx.doi.org/10.5772/54840

Paparo, 2004; Gregori *et al*., 2012). This effect is the consequence of the cooling and/or warming of the shallower layers of the rocks (limestone and dolomia) of the mountain. This cooling or warming involves first the outer layer, and later on the deeper layers. When the body warms up, the outer layer experiences thermal expansion, while it overlies colder and thermally more contracted inner layers. In contrast, when the body cools off, the outer layer shrinks due to thermal compression, while the inner layers are still warm and more expanded. Hence, the outer layers have insufficient room, and some crack will occurs in the outer layer. The phenomenon is the same as what happens to the furniture of a non-heated house, during the cold early-morning hours in winter time. Or this is the same well known phenomenon which typically occurs to rocks in an extreme desert area, etc.

Since, compared to a metal, concrete and bricks have smaller thermal conductivity, the thermoelastic degrading is expected to be comparably more relevant in concrete or brick bridges. And this effect is likely to be maximum when the thermal gradient is comparatively larger during the *cooling* process, i.e. during the early hours of the day. This is the aforementioned effect observed on Gran Sasso.

In contrast, when dealing with a metal structure, a different behavior ought to be observed. The linear elongation of the large metal components of the bridge is the cause of large displacements of the supporting points of every bridge element (during the aforementioned Step 1 of the load test the bridge elongated by 11 mm). This phenomenon ought to be comparatively larger when the absolute value of either the warming or the cooling process is maximum. This maximum (cooling) occurs during the first few hours afternoon. This effect ought therefore to be comparatively more relevant on metal bridges, compared to concrete bridges. This is observed on the Garbatella bridge.

Therefore, whenever temperature records are eventually available during AE monitoring of a bridge, constructed either by concrete or by bricks or by wood or by metal, the temperature gradient ought to be considered, and the response of the AE signal is different depending on the thermal conductivity of the material.

Since violent time-variations of the LF AE signal occurred also during the days when the working activity was totally (or almost totally) absent due to Christmas holiday, the phenomenon ought to be only - or almost only - thermoelastic.

Consider that this thermoelasticity implications were here observed on a bridge in Rome, where a mild and temperate climate is normally enjoyed. The thermoelastic effect has therefore to be expected to be much more important, in terms of ageing hazard, in the case of a bridge located in some comparably more severe environment.

For completeness sake, the HF AE figure analogous to figure 11 is shown in figure 12, which plots raw HF AE data in a *24-hour* cycle diagram. In general, the AE signal was recorded only during the warmer hours of the day, when a thermoelastic effect was active.

Note, however, that after *Dec 16*th, *~ 21 p.m.* through *Dec 17*th *~ 6 a.m*. the viaduct was recovering after the heavy stress of roadbed deposition, and the AE signal was therefore conspicuous.

In addition, during *Dec 24*th, between ~ *21 – 23 p.m.*, some environmental disturbances, i.e. likely wind gusts, caused detectable AE signals.

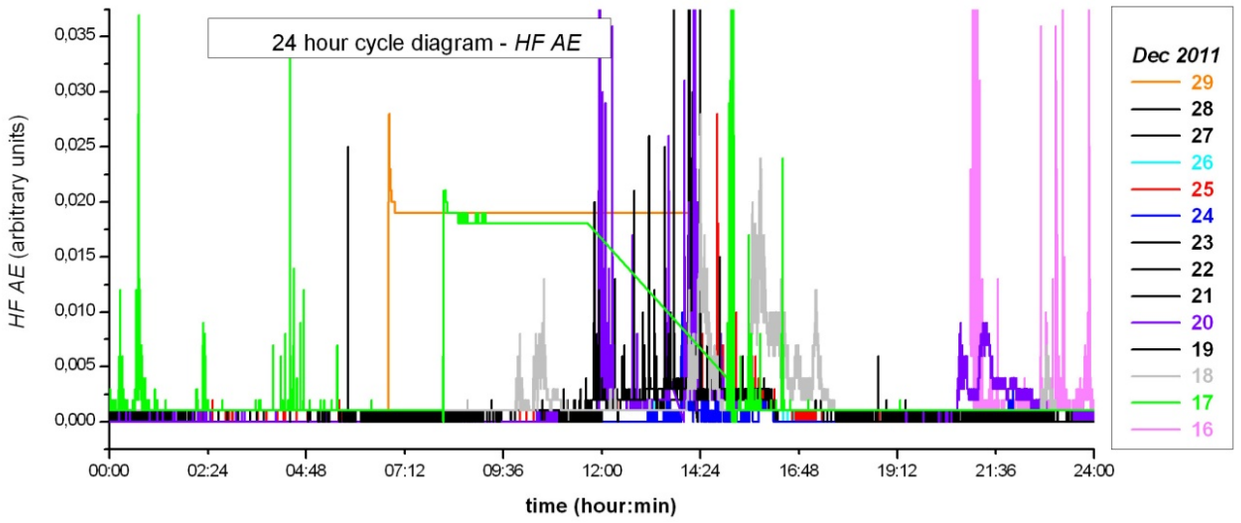

Figure 12. Raw HF AE data, *24-hour* cycle diagram. In general, the AE record were underflow except during the warmer hours of the day, when a thermoelastic effect was active. But, after *Dec 16*th, ~ *21 p.m.* until *Dec 17*th ~ *6 a.m.* the viaduct was recovering after the heavy stress of roadbed deposition, and the AE signal was therefore conspicuous. In addition, during *Dec 24*th, between ~ *21 – 23 p.m.*, some environmental disturbances, i.e. likely wind gusts, produced clearly detectable AE signals.

5.2. Wind gusts

Figure 13 shows a 24 hour cycle diagram of $D_t(t_j)$ of the HF AE *4 sec* data set. Figure 13 displays a comparably confused trend. There is, however, some large effect, which seems thermoelastic. Also the effect of hail is observed (see section 5.5). But, several most prominent disturbances appear uncorrelated either with Sun hours during the day, or also with working days, as during this period of time several days were total holiday. Hence, these disturbances are very likely to be associated with strong wind gusts that frequently, and more or less erratically, occurred during those days in Rome.

Therefore it is reasonable to conclude that wind gusts play a definitely relevant role in metal ageing, even on a bridge that has a structure which is likely to exert a limited aerodynamic opposition to wind.

The plot analogous to figure 13, but referring to LF AE is shown in figure 14, which is shown only for the sake of completeness. But no apparent regularity is observed. The trend appears definitely less influenced by the thermoelastic effect. The excellent performance of the viaduct is shown by the D_t values comprised between ~ *0.6* and *~0.95*. But, during the afternoon some finishing works were being carried out, corresponding to lower D_t values. However, the anomalous low value of D_t occurred between *04:45* and *04:50* LT of *Dec 22*, and it clearly corresponds to a period when the LF AE was constant and underflow. Hence, as mentioned in section 5, it is found $D_t(t_j)=0$.

http://dx.doi.org/10.5772/54840

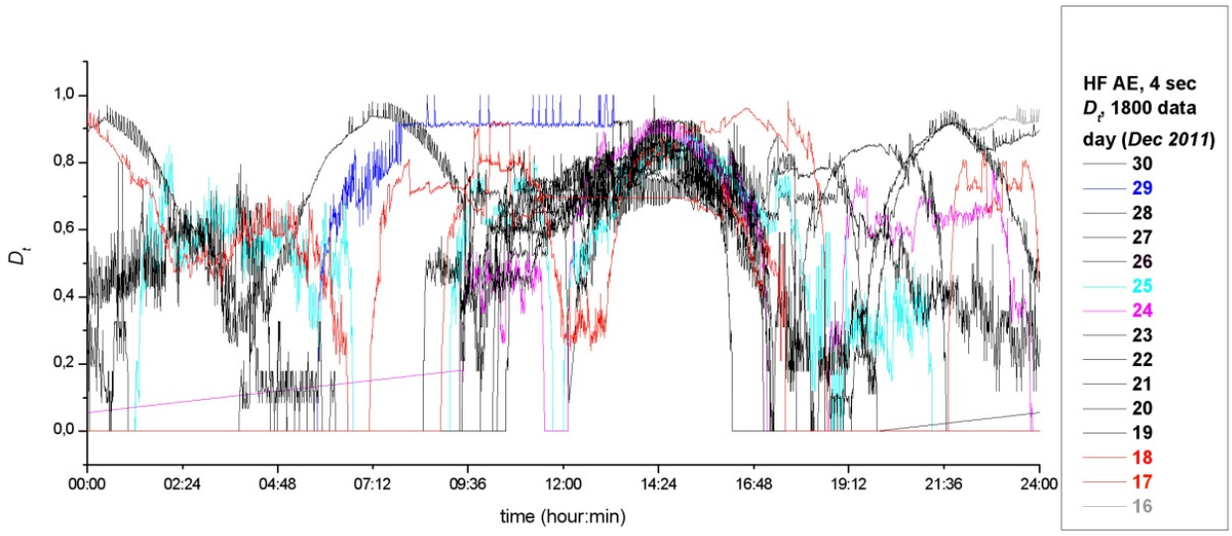

Figure 13. Superposed epoch representation (or "cycle diagram" for *24 hour* period) of D_t HF AE of the *4s* set. Colored lines are the date (*Dec 2011*). No offset was applied. The thermoelastic effect is clearly recognized during the early hours of every afternoon. The violent and erratic oscillations during all other hours of the day are the very likely consequence of strong wind gusts. The flat upper, almost linear, blue trend of *Dec 29* was caused by hail precipitation, and its superposed regular pattern of thin vertical lines is the oscillation of the viaduct at a period *~53.80 sec*. This same oscillation of the viaduct is also displayed like a sequence of thin lines at regular time intervals shown by several other lines in the present diagram. See text.

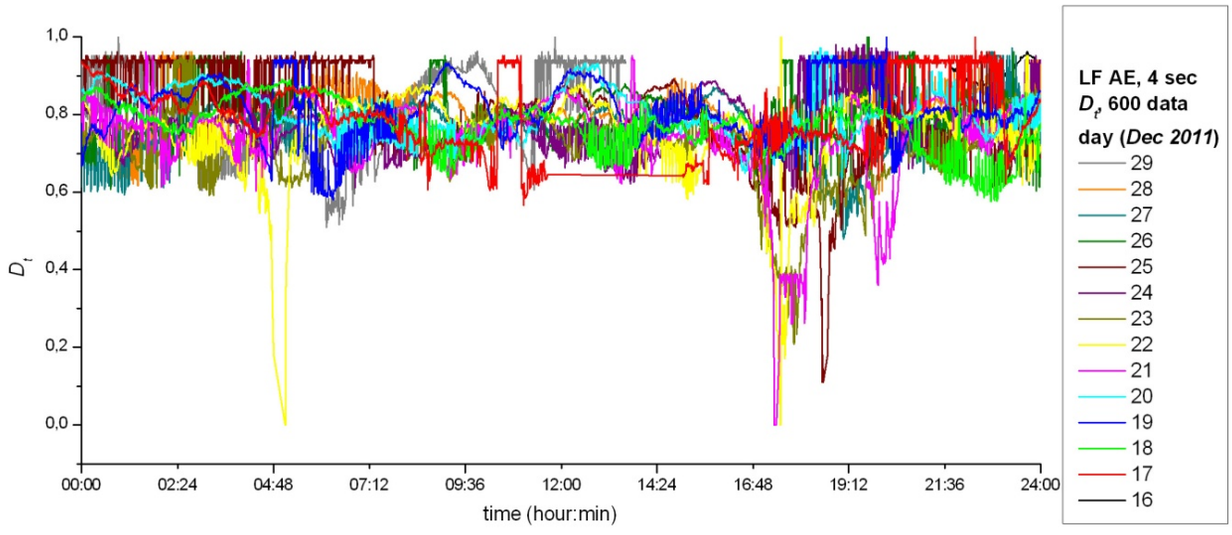

Figure 14. Figure analogous to figure 13, but referring to LF AE. The trend appears definitely less influenced by the thermoelastic effect. The excellent performance of the viaduct is shown by the D_t values comprised between ~ *0.6* and *~0.95*. But, during the afternoon some finishing works were being carried out, corresponding to lower D_t values, or the LF AE signal was underflow. See text.

5.3. Trains

Trains frequently transit under the bridge, moving either slowly (say at $<10\ km/hour$) or faster (say at $\geq 50\ km/hour$).

The disturbance caused on the bridge depends on train speed v according to the following approximate order-of-magnitude estimate. Call m the total mass of displaced matter. If one considers the air blast caused by the train, m is the air mass which is contained inside an air volume equal to the volume of the train. Instead, if one considers the impulse caused by the mass of the train while it crosses on the railway under the viaduct, m is the mass of the train.

In general, it appears more likely to associate the AE disturbance to the shock-wave by air blast, better than to the soil shock caused by train's load. But, if an anemometer is available on the bridge, this dilemma can be promptly solved (see below). In any case, in either case the same following approximate argument can apply.

The impulse on the bridge is proportional to mv, where v is the train speed, and it occurs during a time lag which is roughly proportional to time spent by the train while it crosses under the bridge. If the length of the train is L , this time lag is $\Delta t = L\ /v$. Hence, the intensity of the effect which acts on the bridge may be defined as $F \propto \frac{mv}{\Delta t} = \frac{m}{L} v^2$. Therefore, a train that moves, say, at a speed $\geq 50\ km/hour$ causes an effect which is ≥ 25 times the effect of a train that moves at a speed of $10\ km/hour$.

The effect of the train can be clearly recognized in the *1s* set, but only for HF AE (figure 15), and not in the LF AE (not here shown). This is consistent with the fact that this disturbance is feeble, in terms of consequences on the ageing of the crystalline structures. Hence, only some feeble transient signal is observed and clearly recognized only in HF AE. Differently stated, the disturbance originated by the transit of a train under the bridge is certainly less relevant compared either to wind gusts, or to diurnal thermoelastic effects, or to traffic load.

It is found that urban metro trains produce no sensible effect, as they move very slowly due to their regular stop at the Garbatella station. Only the suburban trains eventually transit at a comparably higher speed, and may cause a detectable effect. Consider also that the train crosses under the bridge at a level which is comparable with the entry of a high-speed train into a tunnel.

According to the official time table, which is reasonably correct (at most apart an error of very few minutes), suburban trains crossed under the bridge at the following times (for comparison purposes, their times have been transformed into day units and decimal fraction of a day). The times of the three trains that caused an HF AE effect are evidenced in bold: 20.50938, **20.51146**, 20.51979, 20.52188, 20.53021, **20.53229**, 20.54063, 20.54271, 20.55104, 20.55313, 20.56007, 20.56146, **20.56701**, 20.57188. The duration of the HF AE disturbance is consistent with the time lag spent by the train to cross underneath the bridge. For instance, a train (say) $\sim 50\ m$ long, moving at $\sim 50\ km/hour$, spends $\sim 1/1000\ hour$ to cross underneath the bridge. Hence, the perturbation originated by the train ought to last $\sim 5 - 10\ sec \sim 0.002$ - $0.003\ hours$. Tick marks in figure 15 are indicated every $0.005\ hours$.

http://dx.doi.org/10.5772/54840

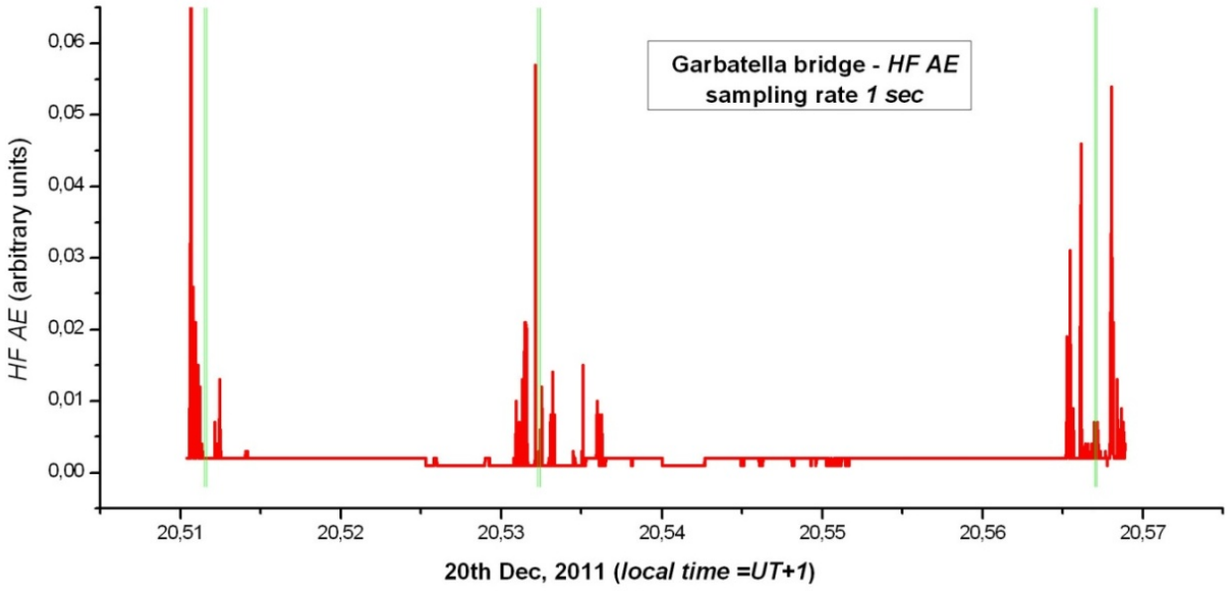

Figure 15. The effect of the train can be clearly recognized in the *1s* set, HF AE. The vertical green lines indicate the times, according to the official timetable, of the transit of every train that is likely to be responsible for an observed HF AE disturbance. Several other trains, with transit time in between these three "fast" trains, caused no HF AE disturbance, and were likely to have a much lower speed. See text.

If the air blast of a train is responsible for this effect, a similar effect ought to be observed for a wind gust. Hence, an anemometer located close to the bridge - and also close to its western terminal, where the railway is located and were the AE records were collected; see figure 1 - should clearly evidence the role of a perturbation on the bridge that is caused either by a wind gust or by a blast-wave by a train.

This datum is interesting for high-speed railways. When a high-speed train (with $v \sim 300-400$ *km/hour*) enters or leaves a tunnel, the impact of its shock-wave is $\sim 900-1600$ times the impact of the shock-wave caused by a train with $v \sim 10$ *km/hour*. This is responsible for a conspicuous ageing of the nacelle of the train. But, the same shock is applied also to the walls of the tunnel, which thus also experiences a corresponding ageing and potential security performance.

5.4. During the load-test

Figure 16 shows $D_t(t_j)$ during load-test. For comparison purposes both HF AE and LF AE are plotted in the present and in the following figures. The correlation appears evident with the sequence of "load-A", "load-B" and "load-C" sets. In particular, while the bridge was recovering after the stress originated by the "load-A" set, a new stress was applied by the "load-B" set, etc.

Figure 17 shows the same plot during a longer time interval, including $D_t(t_j)$ also during *Dec 16*th, when the bridge suffered by a violent stress caused by roadbed deposition.

5.5. Hail

Figure 17 also shows a much anomalous effect close to *Dec 17*th, *10*^{h} *43*^{min} (=*17.44652* in day units). The cause was a short-duration hail storm (according to direct observation by the authors). The effect of hail grains is very small on the crystal bonds of the metal micro-structure of the bridge. While the hail storm is in progress, a tinkle is listened. But the AE transducer can record no audible signal. Rather it measures only HF AE and LF AE released by micro-crystal bonds, which are stressed and broken by hail's impact. However, owing to the very feeble intensity of the effect, the time sequence of the AE records responds essentially only to the timing of different hail grains that hit the bridge at different sites. Hence, since these gentle strokes are essentially random, it must be expected to find $D_t(t_j) \cong 1$, which is indeed observed. Note that other similar $D_t(t_j) \cong 1$ periods of time were observed in those weeks, when additional hail storms occasionally happened in Rome.

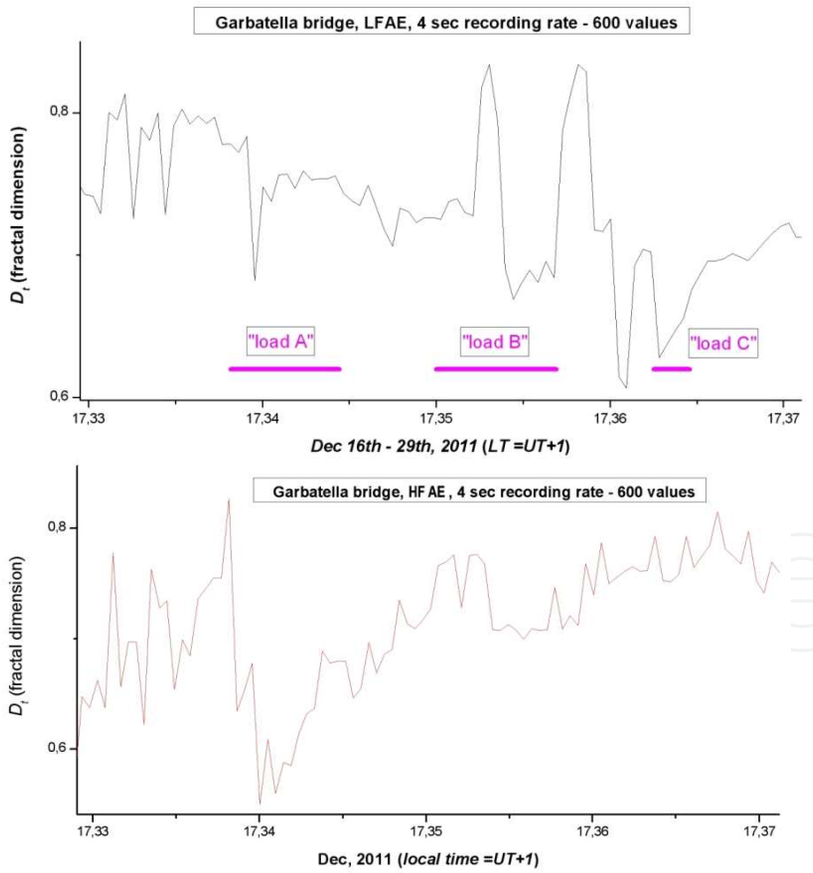

Figure 16. [upper plot] LF AE $D_t(t_j)$ during load-test. The correlation appears evident with the sequence of "load-A", "load-B" and "load-C" sets. [lower plot] HF AE $D_t(t_j)$ during load-test plotted for comparison purpose.

http://dx.doi.org/10.5772/54840

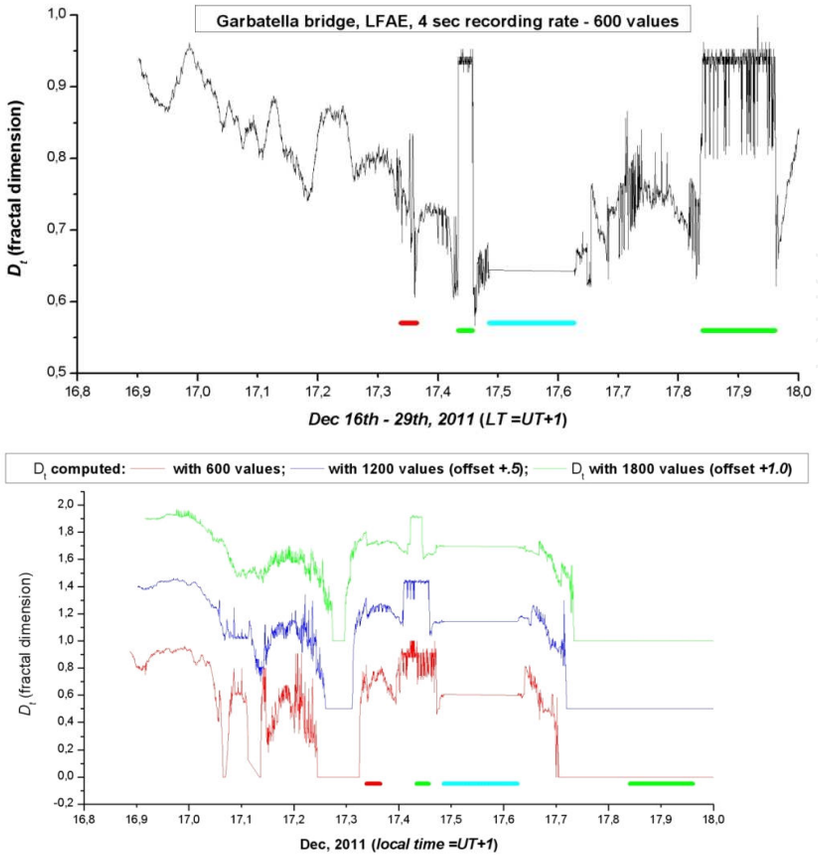

Figure 17. LF AE and HF AE $D_t(t_j)$ until *Dec 18th*. The horizontal bars at the bottom of the two plots indicate: the red bar the time of load test (from its beginning through its maximum load); the light blue bar the period of time with power supply failure; and the green bar the periods of time with hail precipitation. The lack of any $D_t(t_j)$ value for HF AE in the lower plot during the second hail storm (second green line) was caused by instrumental underflow. See text.

6. The proper oscillations of the bridge — The "*arp*" analysis of the outlier series

An interesting inference is derived by means of the "*arp*" of either HF AE's or LF AE's outlier time series, as shown in figures 18 through 21.

In the LF AE (figures 20 and 21) very clear evidence is found for two oscillations, the largest one with period ~ *20.324 min*, and a comparably smaller oscillation at ~ *53.798 sec*.[12] According to model computations, the first 4 proper oscillations of the viaduct, are, in decreasing order, *0.63 Hz*, *1.01 Hz*, *1.23 Hz*, and *1.29 Hz*.

12 In principle, every possible resonance of a viaducts ought to be avoided as far as possible. In this respect, the timing of the cross-lights, which control the access to the viaduct of the surrounding much heavy city-traffic, ought to avoid multiples or submultiples of this period, in order to prevent a possible effect by the impact altogether of a large number of cars on either one 3-lane way of the bridge.

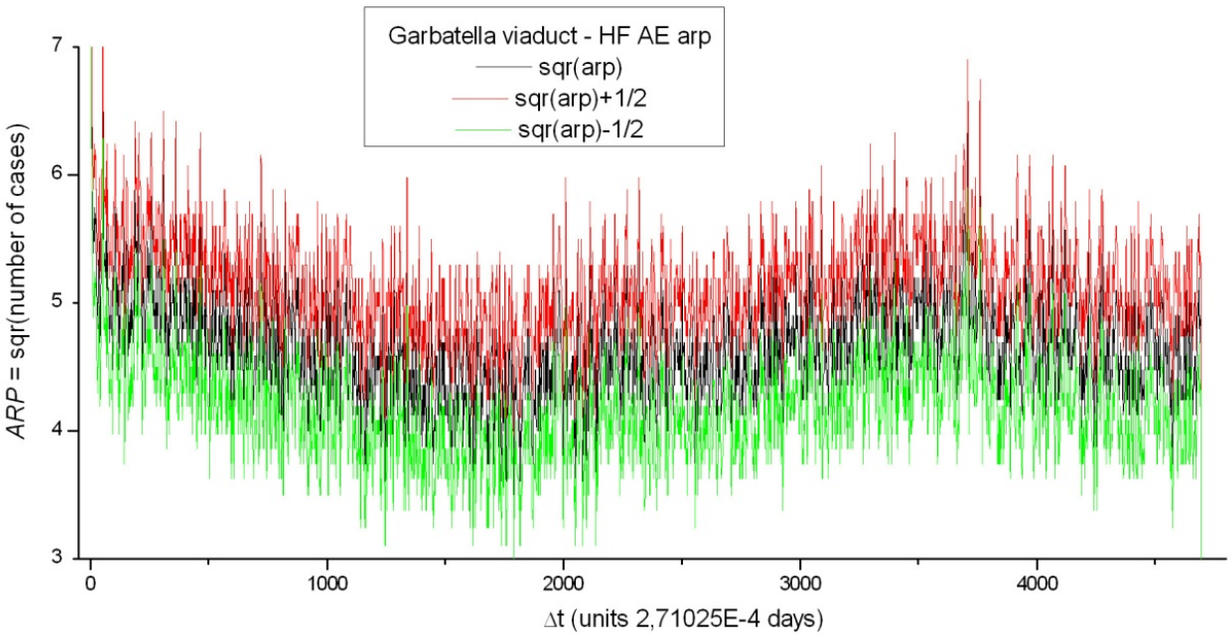

Figure 18. "*Arp*" for HF AE. It displays two major peaks at *1day 7.14348 min* and *1 day 27.43776 min*, respectively.

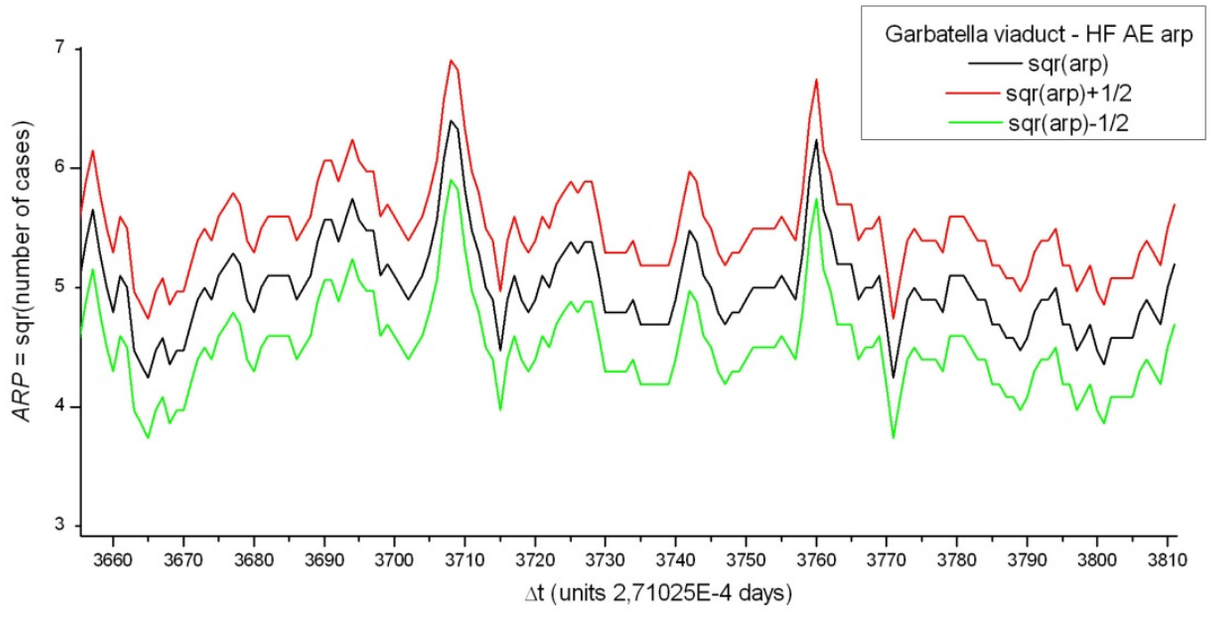

Figure 19. "*Arp*" for HF AE. Detail of figure 18, showing the two major peaks at *1day 7.14348 min* and *1 day 27.43776 min*, respectively.

That is, the two leading oscillation periods inferred by "*arp*" appear much different compared to model computation, although they are a clear and unquestionable observational evidence. On the other hand, consider that with one AE record every *4 sec*, or even every *1 sec*, it is impossible to search for frequencies close to *~1 Hz*. Hence, a much higher time rate in AE

http://dx.doi.org/10.5772/54840

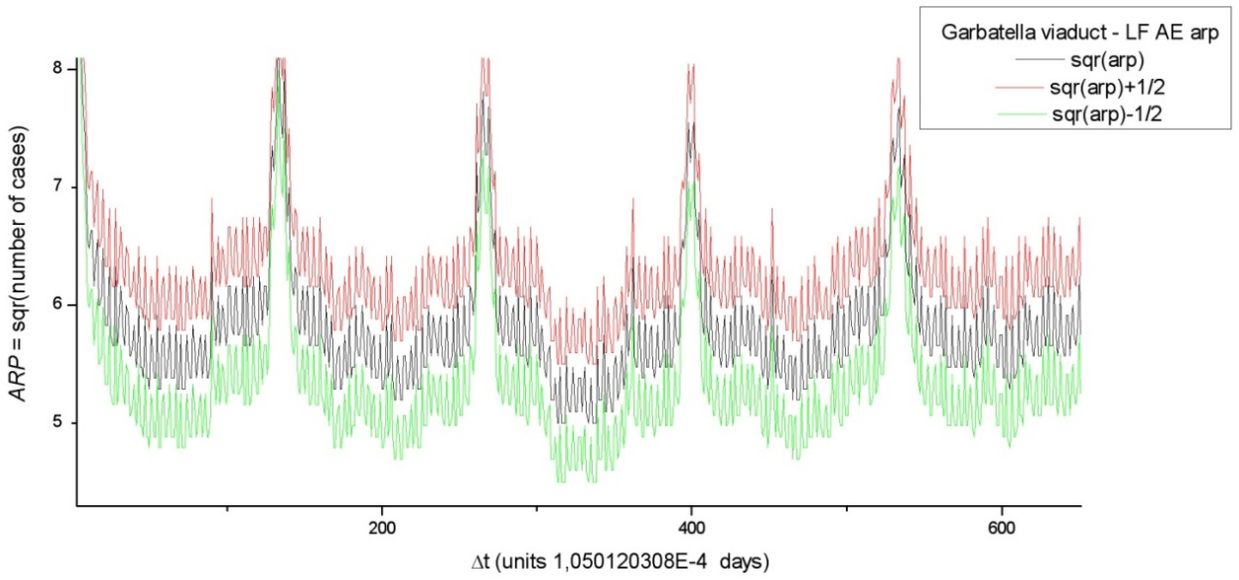

Figure 20. Lesser detail of the "*arp*" for LF AE, showing a major oscillation with period 20.323608 min. The full "*arp*" is not here shown, as it appears much regular and uniform, and it always displays the same periodical pattern.

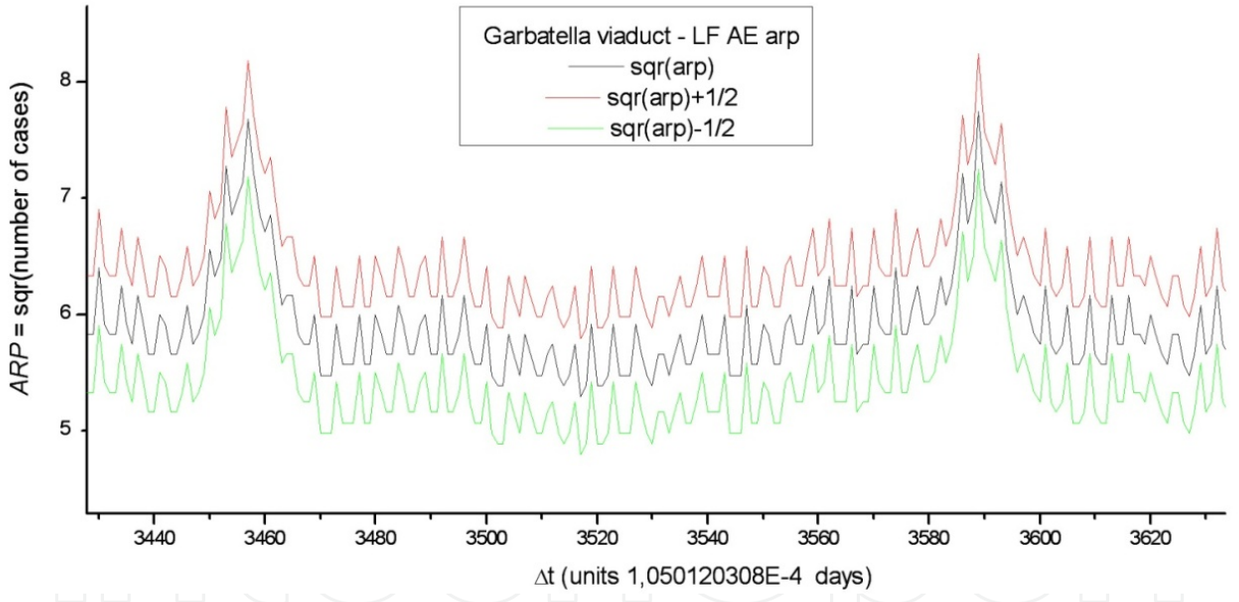

Figure 21. "*Arp*" for LF AE. Detail of the full "*arp*", clearly showing the second major periodicity at *53.7977869 sec*, which is also displayed by the entire "*arp*".

acquisition is strictly required in order to exploit a more pertinent check of the proper oscillation periods of a bridge with model computation.

It should also be pointed out that in the case of a volcano, e.g. of Peteroa (Ruzzante *et al*., 2005, 2008), the analogous "*arp*" plot (unpublished) shows, unlike in the present case history, a dramatic superposition of very many different proper oscillation periods. Indeed, in contrast

to every natural physical system, every manmade structure responds to a specific "simplicity" rationale, according to some ordered geometrical structure, etc.

The ~ *53.798 sec* oscillation is also displayed in figure 13, although superposed over the large disturbances originated by wind gusts or by thermoelastic effects. It is also confirmed by the *1s* data set. Figure 22 shows $D_t(t_j)$ for HF AE of the *1s* set, computed by means of *600, 1200*, and *1800* data. The N_D=*600* case history oscillation appears closely correlated with the transit of the three "fast" crossing trains evidenced in figure 15. The most intriguing feature is evidenced by the N_D=*1800* data case history, which displays a resonance oscillation with a frequency with period ~ 1 *min* (between *59.87 sec* and *61.15 sec*), to be compared with the aforementioned ~ *53.798 sec* oscillation.

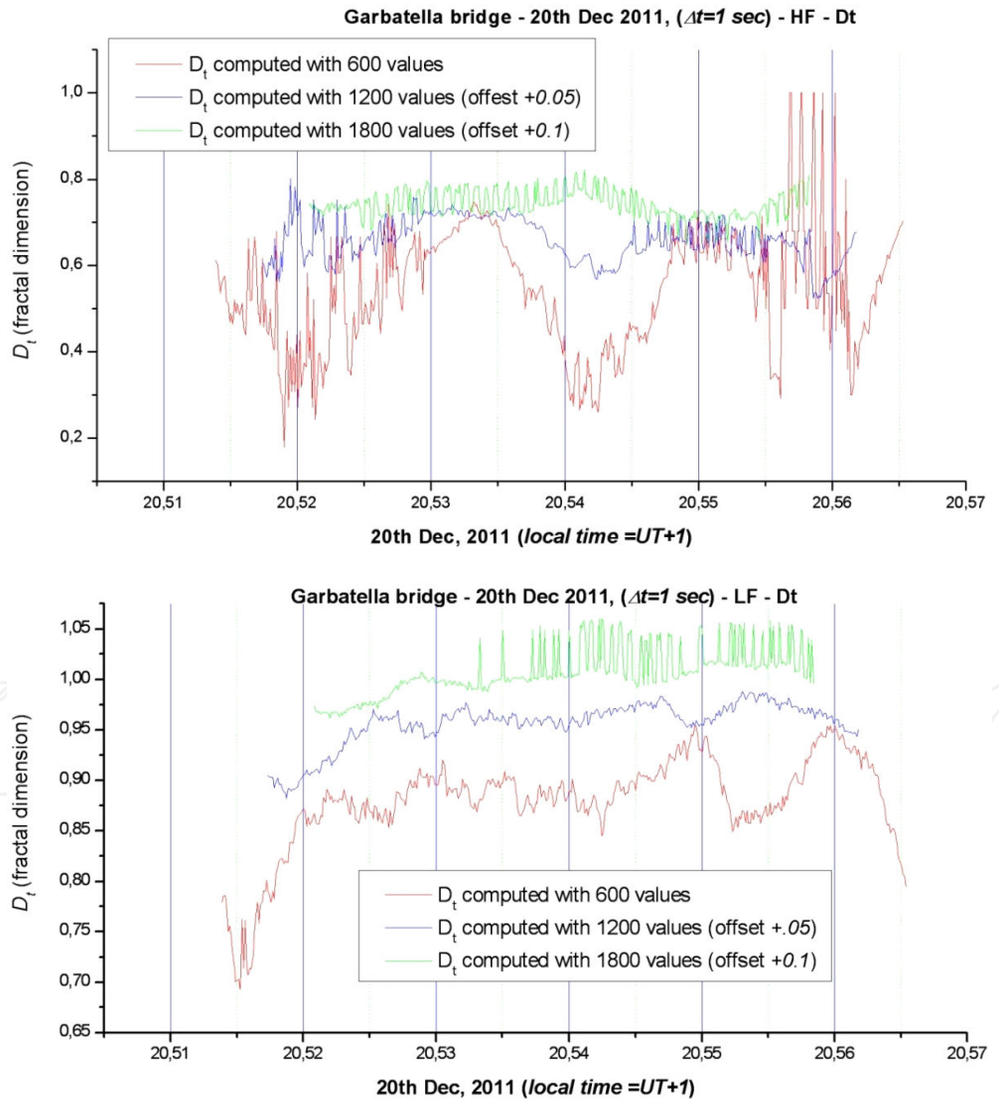

Figure 22. $D_t(t_j)$ for HF AE and LF AE of the *1s* set, computed by means of N_D=*600,* or *1200*, or *1800*.

The same ~ 1 *min* period may be recognized also in the $D_t(t_j)$ LF AE *1s* data series, although only with *1800* data, and with a substantially larger scatter, due to the less faithful LF AE monitoring, compared to the HF AE monitoring, of the external applied disturbance.

In either case, consider that the *1s* set spans a short time interval, and the statistical dependence on N_D results dramatic.

As far as the HF AE are concerned, figures 18 and 19 display a large maximum of "*arp*" corresponding to the diurnal variation (two peaks at *~1 day 7 min*, and *~ 1 day 27 min*) which is evident in figure 6, although it is mainly a consequence of underflow of the AE detecting device. No other intuitively clear periodicities are evidenced, and are to be investigated by a specifically devoted investigation (in preparation).

7. Conclusion

AE monitoring of a metal viaduct appears much effective, feasible, and practical. The same procedure, apart lesser changes in procedures, can be successfully applied also to every concrete or brick or wood bridge.

The recommendations are here summarized, which ought to be taken into account when implementing an AE monitoring on a viaduct.

What parameter should be monitored?

LF AE are certainly much better suited to monitor the overall bridge performance. In general, HF AE may appear comparably less useful. However, HF AE can result important - or sometimes even crucial - whenever a more precise physical interpretation is needed while dealing with some unexpected or unwanted behaviour of materials.

In addition, regular records of meteorological and other environmental parameters ought to be monitored. Also the instant traffic load might be an important environmental information, although, in general, after a suitable calibration carried out once forever, the traffic signal is likely to be easily recognized by a simple routine AE monitoring alone.

What is the recommended time rate?

One rms time-averaged AE record, say, every *25-50 msec* appears to be a good choice, upon considering costs for instruments and data handling, and also the detail which is required in order to detect the proper oscillations of the viaduct.

By this, all kinds of hazard can be safely monitored (except an eventual very rapid damage, such as caused by an explosion, which should require a much higher time rate; but in general this information is of no practical interest).

What is the best procedure for AE monitoring?

In principle, AE monitoring can be operatively planned in three different ways: *(i)* steady permanent real-time monitoring operated from a remote control room; *(ii)* steady permanent monitoring with AE records stored by a data acquisition system, to be later recovered and analyzed; *(iii)* AE test carried out once-in-a-while either periodically or depending on particularly heavy environmental or traffic stress, etc.

The choice of either one procedure, or another, depends on costs and on the specific requirements by the user.

In general, real time remote monitoring may result less expensive, in terms of personnel and of routine automatic operation.

In addition, a once-in-a-while operation cannot be carried out on an instant basis. Indeed, in general one drawback is the time required by the AE recording apparatus to reach regime standard operation. In addition, environmental conditions, such as rain and subsoil water flow, may affect only on some days and not on others the long-term stability of a pillar of a bridge, etc. The same warning applies to every transient disturbance, such as wind gusts which occur only on some days, or a more or less intense diurnal thermal excursion, etc.

In addition, a real-time remote monitoring is also a warranty for a prompt alert about abrupt events that may severely affect the viaduct security (landslides, hurricanes, floods, terrorism, etc.).

How many AE devices are required on a viaduct structure?

In general one AE recording device is needed for every "monolithic" component of the bridge. By "monolithic" component it is here meant a unique solid body through which AE are effectively transmitted. For instance, a metal bridge is a unique huge metal body, and every AE, which is released at any point inside it, is promptly transmitted to all other parts of the bridge with negligible damping (at least as far as the size of the bridge in not exceedingly large).

In addition, the recommendations are to be taken into account provided by structural engineers, who should indicate the nodes that are likely to support the largest stress and are therefore the points that are more likely to suffer by a comparably more rapid ageing.

In any case, a given composite bridge in general has several pillars, and it is likely that AE cannot be easily transmitted from one pillar to the next. Hence, it is necessary to install an AE monitoring on every pillar. The same recommendation holds for every arch. In addition, suitable consideration ought to be given for the connection of a bridge to ground on either one of its sides, mainly whenever there is also a tunnel immediately close to the bridge, etc.

In general, AE monitoring ought to be recommended to be simultaneously operated at different points on the viaduct. However, it is also possible to envisage a periodical AE

http://dx.doi.org/10.5772/54840

test carried out at different times and on different pillars, nodes, etc. Instrumental costs may be reduced, but operational costs may result to be largely increased, and the detail is certainly reduced of the final information about loss of performance and about security.

That is, every case history has to be considered independently, and the costs for implementation and operation are to be optimized depending on the required kind of alert which is required by the user.

What is the relevant difference between a metal viaduct and a concrete or brick or wood viaduct?

The aforementioned "monolithic" component structure has to be taken into account when dealing with every kind of viaduct.

Concrete bridges are expected to suffer by the comparative more intense thermoelastic effect during the early hour of a cold morning, unlike metal bridges that suffer by thermal excursion mainly during the hotter hours of the day.

A present great concern deals with the unknown performance of concrete, when it is older than one century, mainly when its ageing is combined with the effect of some particularly hostile environment.

Brick bridges ought to be tested in order to assess how far AE can be transmitted between contiguous bricks depending on the specific kind of mortar that was used. In general, a brick wall has a much compact structure, and in general AE transmission is likely to result much effective. In addition, in general a wetting of materials may dramatically improve AE transmission, etc. Hence, every case history has to be suitably evaluated, and every aforementioned warning has to be considered, which also applies to metal or concrete bridges.

Wood bridges require no particular additional warning, other than the investigation and calibration of that specific kind of wood, when it is strained by an applied stress. Compared to metal or concrete or stone etc., wood behaves much differently depending on its fibrous structure, which determines its "elastic" or "plastic" response, and also some kind of comparably time-delayed final yielding and rupture.

Acknowledgements

We thank Ing. Francesco Del Tosto for kindly providing us with some information about the height of the viaduct with respect to the railway, and about the preliminary activity on the bridge, carried out on *December 16th*, the day preceding the load test. We thank Ing. Fabio Rocchi for kindly providing us with the official documentation and drawings dealing with the load test of the viaduct.

Author details

Giovanni P. Gregori[1,2,3], Giuliano Ventrice[1,4,5], Sebastiano Pinori[1,6], Genesio Alessandrini[1,6] and Francesco Bianchi[1,7]

*Address all correspondence to: giovanni.gregori@sme-ae-it

1 S.M.E. (Security, Materials, Environment) s.r.l., Roma, Italy

2 IEVPC – International Earthquake and Volcano Prediction Center, USA

3 IDASC(CNR), Roma, Italy

4 PME Engineering (Progettazione Macchine Elettroniche), Italy

5 SAE-Technology (System Acoustic Emission Technology), Italy

6 "Più s.r.l. costruire il futuro"- Gruppo Alessandrini, Italy

7 Faculty of Architecture, Third University of Rome, Italy

References

[1] Biancolini, M. E., Carlo Brutti, Gabriele Paparo, Alessandro Zanini, 2006. Fatigue cracks nucleation on steel, acoustic emission and fractal analysis. *Int. J. Fatigue*, 28, (12), 1820-1825.

[2] Braccini, S., C. Casciano, F. Cordero, F. Frasconi, G. P. Gregori, E. Majorana, G. Paparo, R. Passaquieti, P. Puppo, P. Rapagnani, Fulvio Ricci, and R. Valentini, 2002. Monitoring the acoustic emission of the blades of the mirror suspension for a gravitational wave interferometer. *Phys. Lett. A*, 301, 389-397.

[3] Cello, Giuseppe, 2000. A quantitative structural approach to the study of active fault zones in the Apennines (peninsular Italy), *J. Geodyn*., 29, 265-292.

[4] Cello, Giuseppe, and B. D. Malamud, (eds), 2006. Fractal analysis for natural hazards, *Geol. Soc. Lond., Spec. Publ.*, 261, 1-172.

[5] Gregori, Giovanni P., and Gabriele Paparo 2006. The Stromboli crisis of 28÷30 December 2002. *Acta Geod. Geophys. Hung.*, 41, (2), 273-287.

[6] Gregori, Giovanni P., and Gabriele Paparo, 2004. Acoustic emission (*AE*). A diagnostic tool for environmental sciences and for non destructive tests (with a potential application to gravitational antennas), in *Schröder (2004)*, 166-204.

[7] Gregori, Giovanni P., Gabriele Paparo, Maurizio Poscolieri, and Alessandro Zanini, 2005. Acoustic emission and released seismic energy. *Natural Hazards Earth System Sci.*, 5, 777-782.

[8] Gregori, Giovanni P., Gabriele Paparo, Maurizio Poscolieri, Claudio Rafanelli, and Giuliano Ventrice, 2012. Acoustic emission (AE) for monitoring stress and ageing in materials, composing either manmade or natural structures, and their precursors. In *Sikorski (2012)*, 365-398.

[9] Gregori, Giovanni P., Gabriele Paparo, Ugo Coppa, and Iginio Marson, 2002. Acoustic emission in geophysics: a reminder about the methods of analysis. *Boll. Geofis. Teor. Appl.*, 43, (1/2), 157-172.

[10] Gregori, Giovanni P., Matteo Lupieri, Gabriele Paparo, Maurizio Poscolieri, Giuliano Ventrice, and Alessandro Zanini, 2007. Ultrasound monitoring of applied forcing, material ageing, and catastrophic yield of crustal structures. *Nat. Hazards Earth Syst. Sci.*, 7, 723-731.

[11] Gregori, Giovanni P., Maurizio Poscolieri, Gabriele Paparo, Sara De Simone, Claudio Rafanelli, and Giuliano Ventrice, 2010. "Storms of crustal stress" and AE earthquake precursors, *Nat. Hazards Earth Syst. Sci.*, 10, 319–337.

[12] Guarniere, Salvatore, 2003. L'emissione acustica come strumento diagnostico di strutture a varia scala. *Unpublished PhD Thesis*, 144 pp., University of Messina, Messina, Italy.

[13] Kapteyn, Jacobus Cornelius, 1903. *Skew frequency curves in biology and statistics*, Astronomical Laboratory, Noordhoff, Groningen.

[14] Kapteyn, Jacobus Cornelius, 1912. Definition of the correlation - coefficient. *Month. Not. Roy. Astr. Soc.*, 72, 518-525.

[15] Kapteyn, Jacobus Cornelius, and Marie Johan van Uven, 1916. *Skew frequency-curves in biology and statistics*, 69 pp., Hoitsema Brothers, Groningen.

[16] Lagios, Evangelos, Vassilis A. Sakkas, Issaak Parcharidis, Maurizio Poscolieri, Giovanni P. Gregori, Gabriele Paparo, and Iginio Marson, 2004. Ground deformation deduced by *DGPS*, *DInSAR*, *AE*, and *DEM* analysis in Cephallonia Island, presented at the *SCI 2004* congress, *The 8th World Multi-Conference on Systemics, Cybernetics and Informatic,* Orlando (Florida) 18-21 July, 6 pp.

[17] Paparo, Gabriele, and Giovanni P. Gregori, 2003. Multifrequency acoustic emissions (*AE*) for monitoring the time evolution of microprocesses within solids. *Reviews of Quantitative Nondestructive Evaluation*, 22, (*AIP Conference Proceedings* ed. by D. O. Thompson and D. E. Chimenti), 1423-1430.

[18] Paparo, Gabriele, Giovanni P. Gregori, Alberto Taloni, and Ugo Coppa, 2004. Acoustic emissions (*AE*) and the energy supply to Vesuvius – 'Inflation' and 'deflation' times. *Acta Geod. Geophys. Hung.*, 40, (4), 471-480.

[19] Paparo, Gabriele, Giovanni P. Gregori, Francesco Angelucci, Alberto Taloni, Ugo Coppa, and Salvo Inguaggiato, 2004a. Acoustic emissions in volcanoes: the case histories of Vesuvius and Stromboli. In the *Proceedings of the SCI 2004 meeting*, Orlando, Florida, July 2004.

[20] Paparo, Gabriele, Giovanni P. Gregori, Maurizio Poscolieri, Iginio Marson, Francesco Angelucci, and Giorgia Glorioso, 2006. Crustal stress crises and seismic activity in the Italian peninsula investigated by fractal analysis of acoustic emission (*AE*), soil exhalation and seismic data. In *Cello and Malamud (2006)*, 47-61.

[21] Paparo, Gabriele, Giovanni P. Gregori, Ugo Coppa, Riccardo de Ritis, and Alberto Taloni, 2002. Acoustic emission (*AE*) as a diagnostic tool in geophysics. *Annals of Geophysics*, 45, (2), 401-416.

[22] Poscolieri, Maurizio, Evangelos Lagios, Giovanni P. Gregori, Gabriele Paparo, Vassilis A. Sakkas, Issaak Parcharidis, Iginio Marson, Konstantinos Soukis, Emmanuel Vassilakis, Francesco Angelucci, Spyridoula Vassilopoulou, 2006. Crustal stress and seismic activity in the Ionian archipelago as inferred by combined satellite and ground based observations on the Kefallinìa Island (Greece). In *Cello and Malamud (2006)*, 63-78.

[23] Poscolieri, Maurizio, Giovanni P. Gregori, Gabriele Paparo, and Alessandro Zanini, 2006a. Crustal deformation and *AE* monitoring: annual variation and stress-soliton propagation, *Nat. Hazards Earth Syst. Sci.*, 6, 961-971.

[24] Ruzzante, Josè, and Maria Isabel Lòpez Pumarega, (eds), 2008. *Acoustic emission,* Vol. 1, *Microseismic, learning how to listen to the Earth…*, 68 pp., CNEA, Buenos Aires. ISBN 978-987-05-4116-5.

[25] Ruzzante, José, Gabriele Paparo, Rosa Piotrkowski, Maria Armeite, Giovanni P. Gregori, and Isabel Lopez, 2005. Proyecto Peteroa, primiera estaciòn de emisiòn acustica en un volcàn de los Andes, *Revista de la Uniòn Iberoamericana de Sociedades de Fìsica*, 1, (1), 12-18.

[26] Ruzzante, Josè, Maria Isabel Lòpez Pumarega, Giovanni P. Gregori, Gabriele Paparo, Rosa Piotrkowski, Maurizio Poscolieri, and Alessandro Zanini, 2008. Acoustic emission (*AE*), tides and degassing on the Peteroa volcano (Argentina). In *Ruzzante and Lòpez Pumarega (2008)*, 37-68.

[27] Schröder, Wilfried, (ed.), 2004. Meteorological and geophysical fluid dynamics (A book to commemorate the centenary of the birth of Hans Ertel), 417 pp., *Arbeitkreis Geschichte der Geophysik und Kosmische Physik*, Wilfried Schröder/Science, Bremen.

[28] Sikorski, Wojciech, (ed.), 2012. *Acoustic emission*, 398 pp., InTech; *http://www.intechopen.com/articles/show/title/acoustic-emission-ae-for-monitoring-stress-and-ageing-in-materials-including-either-manmade-or-natur*; ISBN 978-953-51-0056-0.